Physics – Uspekhi **67** (2) 129 – 156 (2024)

REVIEWS OF TOPICAL PROBLEMS

PACS numbers: 42.55.Wd, **42.65. – k**, **42.81. – i**

40th ANNIVERSARY OF THE PROKHOROV GENERAL PHYSICS INSTITUTE, RUSSIAN ACADEMY OF SCIENCES

Hollow-core optical fibers: current state and development prospects

A D Pryamikov, A V Gladyshev, A F Kosolapov, I A Bufetov

DOI: https://doi.org/10.3367/UFNe.2023.12.039616

Contents

1. Introduction **129**
1.1 Classification of hollow-core optical fibers according to mechanisms of light localization in the core; 1.2 Technology of fabricating hollow-core optical fibers
2. Revolver optical fiber as the basis of promising optical communication lines **136**
3. Transporting radiation with high mean and/or peak power **137**
3.1 Properties of standard and hollow-core optical fibers: a comparison; 3.2 Propagation of optical discharge through a revolver optical fiber
4. Nonlinear optics in gas-filled hollow-core optical fibers **142**
4.1 Nonlinear compression and generation of ultrashort laser pulses in hollow-core optical fibers; 4.2 Gas fiber lasers and mid-infrared range development; 4.3 Studies of gas discharge fiber lasers; 4.4 First gas discharge fiber laser
5. Conclusion **153**
References **154**

Abstract. The history of the development and current state of hollow-core optical fibers are reviewed. The basic properties which determine the competitive advantages of hollow-core fibers and promising areas for their practical application are discussed. Recent advances in reducing optical losses and the prospects for telecommunication applications of hollow-core fibers, issues of transporting high-intensity optical radiation, and results on nonlinear compression and the generation of ultrashort pulses in gas-filled hollow-core fibers are reviewed. A separate section is devoted to the latest achievements in the development of gas fiber lasers using both optical radiation and gas discharge for pumping.

Keywords: fiber optics, hollow-core optical fibers, nonlinear fiber optics

1. Introduction

Optical fibers have become an integral part of our lives. In the modern information society, they actually form a living environment that has become so familiar and natural that most of us do not even notice it, like air in everyday life. However, when using the Internet for work, shopping online, communicating on social networks, or participating in video conferences, we often use optical fibers, despite the illusion of its absence created by wireless access technologies. Moreover, based on optical fibers, compact, stable, and reliable sources of laser radiation are being developed, which have found numerous applications from industrial material processing to biomedicine and even the search for new exoplanets.

Such success of optical fibers is largely due to the properties of fused silica, which is the basic material used to fabricate both the cladding and the core of optical fibers. The technology of optical fiber production based on fused silica has been developing for more than 40 years and during that time many of the parameters have reached their fundamental limits. For example, the absolute minimum of optical losses in optical fibers, determined by such fundamental mechanisms as Rayleigh scattering and phonon absorption in fused silica, amounts to ~ 0.15 dB km^{-1} at a wavelength of 1.56 μm and has already practically been reached. It is also well known that such fundamental mechanisms as absorption by electrons and phonons make it impossible to use fused silica in the ultraviolet (UV) and mid-infrared (IR) ranges, respectively. However, there is permanent demand for further development of optical fibers beyond the limits set by the properties of fused silica.

An elegant solution to the problem is hollow-core fibers (HCFs), in which the radiation field is localized in the hollow core. The hollow core is by default air-filled but can be vacuumized or filled with other gases with the desired optical properties.

The development of hollow-core fibers followed the path of minimizing the proportion of optical power propagating in the cladding. Since 1999, when the first HCFs with a photonic band gap were created [1], this proportion has been reduced from $\sim 10^{-2}$ to $\sim 10^{-5}$ thanks to the invention of antiresonant hollow-core fibers possessing a negative curvature of the cladding–core boundary [2–4]. The extremely weak interac-

A D Pryamikov, A V Gladyshev, A F Kosolapov, I A Bufetov (*)
Prokhorov General Physics Institute, Russian Academy of Sciences,
Dianov Fiber Optics Research Center,
ul. Vavilova 38, 119333 Moscow, Russian Federation
E-mail: (*) iabuf@fo.gpi.ru

Received 11 August 2023, revised 12 December 2023
Uspekhi Fizicheskikh Nauk **194** (2) 138 – 168 (2024)
Translated by V L Derbov

tion of radiation localized in the hollow core with the fiber cladding largely allows avoiding the limitations imposed by the cladding material. Thanks to this fact, hollow-core fibers can demonstrate high radiation resistance to both high-intensity optical radiation and ionizing radiation. In addition, HCF technology holds a promise to overcome the fundamental optical loss limit in telecommunication optical fibers, as well as broaden the spectral range available for hollow-core fibers, the cladding of which is made according to well-known and developed fused silica technology.

In recent years, several reviews on the properties and applications of hollow fibers have been published in the foreign literature [5–9]. However, in Russian scientific journals, this topic is presented only fragmentarily and lags behind the current level of development of hollow-core fibers.

In the present review, we try to fill this gap. This review presents the history of the development, basic properties, and fundamentals of the technology of hollow-core fibers (Section 1), as well as discusses the results of HCF studies in the most actively progressing spheres. Considered are such issues as reducing optical losses and telecommunication applications of HCFs (Section 2), transporting high-intensity optical radiation (Section 3), nonlinear compression and the generation of ultrashort pulses (Section 4.1), and the development of gas fiber lasers, including the creation of the first gas discharge fiber laser (Sections 4.2–4.4).

1.1 Classification of hollow-core optical fibers according to mechanisms of light localization in the core

The main characteristic of a guided mode propagating as a traveling wave $\exp[\mathrm{i}(\beta z - \omega t)]$ along the core of a hollow-core optical fiber (z-axis) is its propagation constant $\beta = \omega n_{\mathrm{eff}}/c$. This formula, in addition to the radiation frequency ω and the speed of light in a vacuum c, includes the effective refractive index n_{eff}, which is obtained by solving an eigenvalue problem for the electromagnetic field of the modes of the considered HCF with the boundary conditions taken into account. The main difference among all types of HCF eigenmodes and eigenmodes of optical fibers that localize radiation based on the principle of total internal reflection is the presence of imaginary part $n_{\mathrm{eff}} = \mathrm{Re}\,(n_{\mathrm{eff}}) + \mathrm{i}\,\mathrm{Im}\,(n_{\mathrm{eff}})$ in the HCF modes. This means that the HCF eigenmodes are leaky and lose energy as they propagate. Sometimes it is also said that there is coupling between the hollow core modes and the cladding modes, which can be considered separately as spatial channels of energy transfer. Due to exactly this coupling, the leakage of energy from the modes of the air-filled core occurs. The real part $\mathrm{Re}\,(n_{\mathrm{eff}})$ of the effective refractive index determines the phase of the HCF core mode, whereas the imaginary part $\mathrm{Im}\,(n_{\mathrm{eff}})$ determines the losses of this mode. It is worth noting that the losses of the hollow core mode include both the wave-guiding part related to the specific design features of the fiber cladding and the purely material losses in the HCF cladding. Thus, successful propagation of radiation in a hollow core requires a search for such a design of the HCF cladding that would minimize the magnitude of the imaginary part of n_{eff}.

The concept of hollow-core fibers for long-range transmission of radiation began its development with Ref. [10], which proposed the simplest HCF design with no cladding at all. It was a cylindrical tube with an air-core in an infinite dielectric medium. The mode radiation of such an HCF merely refracted at the boundary of the air-core and went to infinity. Such a wave-guiding system could be calculated almost analytically, and only the final dispersion equations had to be solved numerically to determine n_{eff} for the modes of the air-core. Calculations showed that wave-guiding losses in such HCFs are proportional to the ratio $\sim \lambda^2/R^3$, where λ is the wavelength and R is the radius of the air-core of the HCF. For example, this type of HCF made of glass with refractive index $n = 1.5$ at a wavelength of $\lambda = 1$ μm has losses of 1.55 dB km^{-1} for the EH_{11} mode for the air-core radius $R = 1$ mm. In the presence of a bend with curvature radius $R_{\mathrm{bend}} \sim 10$ km, the HCF losses double, which, in the opinion of the authors, made it impossible to use HCFs of a dielectric material for long-range transmission of radiation. In addition, it should be borne in mind that HCFs with such a large radius of the air-filled core would be essentially multimode.

An important step towards solving the problem of using hollow-core fibers to transmit radiation with low losses was the use of the anti-resonance phenomenon. Theoretically, the band structure of radiation transmission in capillaries with walls of finite thickness was demonstrated in Ref. [11]. In this paper, the authors analytically derived the formulas for the capillary wall thickness values, corresponding to high-efficiency radiation transmission through or reflection from this wall. The terms 'antiresonant fiber' and 'antiresonant mechanism of radiation localization in a fiber' were used for the first time in experimental paper [12]. The presence of band gaps was demonstrated theoretically and experimentally for radiation propagating in a planar optical waveguide having a 4-μm-thick core of pure SiO_2 with air on one side and a silicon layer on the other side. Based on Snell's law, the anti-resonance condition was analytically derived, under which the coefficient of reflection from the above planar layers is maximum. It was shown that in fact they can be considered an analog of the Fabry–Perot interferometer. As to circular HCFs made of fused silica and HCFs with antiresonant dielectric coatings on the inner surface of the core boundary, the first samples of such fibers were fabricated and demonstrated in Refs [13, 14]. In Ref. [13], the problem of transmitting the radiation of a CO_2 laser through an HCF with a metallic or metal-dielectric coating on the inner surface of a circular wave-guiding tube was studied. In the case of a dielectric coating on a metallic layer on the inner surface of an air-filled core, the HCF can be thought of as guiding radiation partially due to the anti-resonance mechanism. Reference [14] also considered the transmission of radiation at a wavelength of 10.6 μm, but in silica glass tubes with diameters of 1.04 mm and 2 mm. The experimentally measured losses in a straight HCF amounted to 1.9 dB m^{-1} and 0.69 dB m^{-1}, respectively, the losses calculated according to the theory [10] being in not bad agreement with these values. The main problem that arises when transmitting radiation at such diameters of the air-filled core is great losses due to the HCF bending. A complete description of the problems related to the transmission of radiation in the mid-IR spectral region through HCFs with a large diameter of the hollow core and metal–dielectric coating of its inner surface requires mentioning the studies by Prof. Harrington [15], who reported the transmission of radiation from a CO_2 laser at a wavelength of 10.6 μm with losses of 0.1 dB m^{-1} bent with a radius of 5 cm. CO_2 laser radiation transmission with a power of up to 3 kW was also demonstrated. As was mentioned, all the above HCFs had a circular air-core with radius $R \gg \lambda$, coated either with a layer of metal like silver, or additionally with a dielectric layer. The

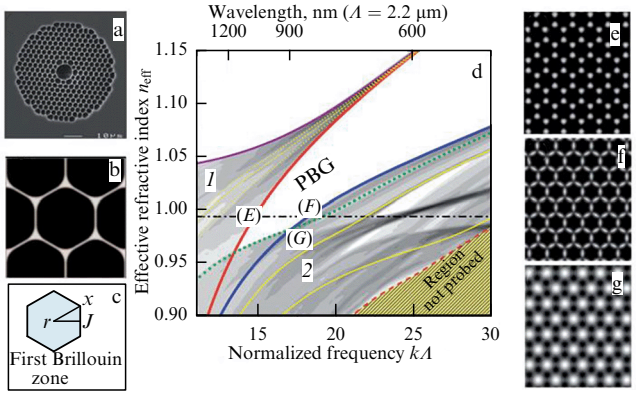

Figure 1. (a) Cross section of a photonic-crystal HCF; (b, c) individual element of the cladding of the photonic-crystal HCF and the first Brillouin zone, determining the structure of the photonic band gap of the HCF cladding; (d) photonic band gap (PBG) of the photonic-crystal HCF and the structure of bands, in which radiation of the HFC air-filled core mode is coupled with modes of the photonic-crystal cladding of various types (e–g). In the figure, $k = 2\pi/\lambda$, where λ is the wavelength; Λ is the distance between the centers of air cells of the HCF cladding (b). (Adopted from Ref. [17].)

mechanism of reflecting radiation from a dielectric film is well explained in terms of the antiresonant model, and it is sufficient to apply the ray optics approach to describe it theoretically. The main drawbacks of these HCFs are the great sensitivity to bending due to the large core diameter and the multimode operation. Moreover, the level of losses in such HCFs is always no less than ~ 0.1 dB m^{-1}.

Considerable progress in the development of new types of HCFs began with the invention of the first microstructured or photonic-crystal HCF [1]. The basis for creating this type of HCF was the hypothesis of Prof. Russell that the localization of light in the air-core of an HCF is possible because of photonic band gaps that arise in the cladding, implemented as a two-dimensional photonic crystal [16]. In this case, a two-dimensional photonic crystal has a hexagonal packing of air-filled holes circular-shaped in the HCF cladding cross section. Numerical calculations showed that, in this case, for HCF modes with the effective refractive index $n_{eff} < 1$, there is an interval of Δn_{eff} in which the photonic band gaps can merge for radial and azimuthal directions of radiation propagation in the HCF cross section. This allows localizing the modes in the air-core.

Figure 1 shows the cross-section structure of a photonic-crystal HCF, its Brillouin zone, and the modes of the photonic-crystal cladding that determine the structure of the photonic band gap (PBG). From Fig. 1, it is seen that the effective width of the PBG is determined by the spectral density of modes of photonic-crystal claddings of various types (Fig. 1e–g). Obviously, with such a complex structure of the photonic-crystal cladding, it is hard to obtain a wide PBG for the transmission of the air-core modes. Various types of microresonators in the cladding of such HCFs significantly reduce the spectral transmission band of the air-core modes. This is one of the main drawbacks of photonic-crystal HCFs. Nevertheless, in such HCFs, low loss at a level of ~ 1.2 dB km^{-1} was reached when transmitting the radiation at a wavelength of 1.55 μm [18]. Further loss reduction appeared impossible because of both the specific optical properties of the photonic-crystal cladding and the boundary shape of the air-core (the importance of the HCF core boundary shape will be explained below), and the roughness arising on the inner surface of the air-filled core in the process of HCF drawing [18]. In this case, it was pointed out that the scattering losses due to such roughness depend on the wavelength λ as $\sim 1/\lambda^3$. This also became an obstacle for making this HCF of fused silica and high-purity synthetic silica operating in the mid-IR spectral range [19, 20]. In this case, the overlap of the transverse distribution of the air-filled core modes with the HCF cladding is critical because of the growth of the fused silica material losses in the mid-IR range. The best results in terms of losses for photonic-crystal HCFs in the single-mode regime were 2.6 dB m^{-1} at a wavelength of 3.13 μm [19] and 0.13 dB m^{-1} at a wavelength of 3.33 μm [20].

The problem of insufficiently wide transmission bands in photonic-crystal HCFs was solved with the appearance of a new type of hollow-core optical fiber, namely HCFs with Kagomé cladding (Fig. 2). In this HCF, the air-filled core

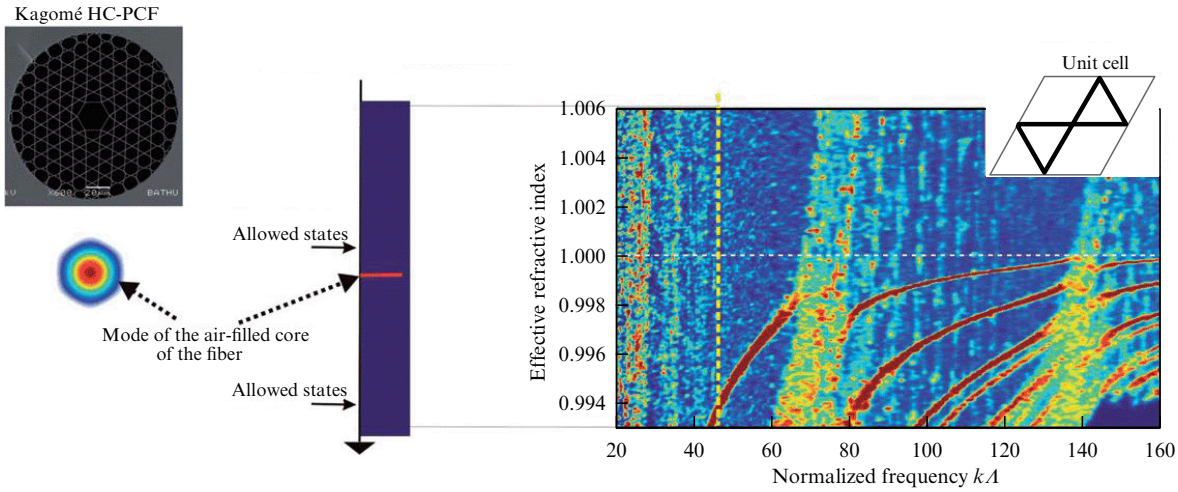

Figure 2. Cross section of a photonic-crystal HCF with Kagomé cladding for transmitting radiation in broad transmission spectral bands. Radiation localization mechanism in this HCF, where the air-core mode exists in the continuum of the modes of photonic-crystal cladding. White dashed line corresponds to $n_{eff} = 1$, red lines and dots show dispersion dependences of the HCF cladding modes. Inset shows a unit cell of the HCF cladding. (Adopted from Ref. [17].)

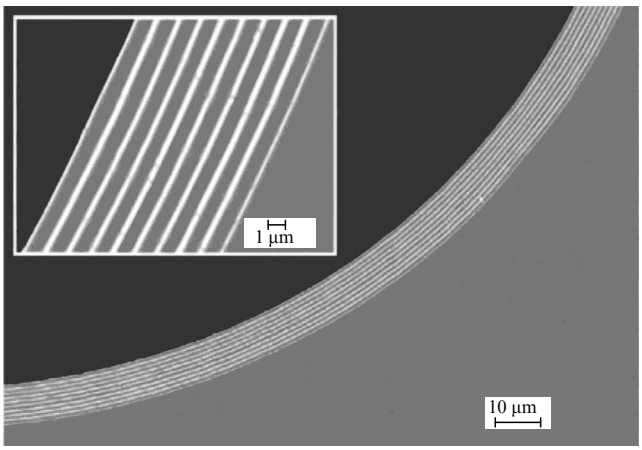

Figure 3. Cross section of the cladding of a Bragg HCF intended to transmit radiation in the mid-IR range of the spectrum. (Adopted from Ref. [23].)

mode with $n_{\text{eff}} < 1$ lies in a certain quasicontinuum of the cladding modes (see Fig. 2); however, even when their dispersion curves intersect, $n_{\text{core}}(\lambda) \approx n_{\text{cladd}}(\lambda)$ (i.e., in the case of phase matching), the coupling of these modes is negligibly small. As is seen from Fig. 2, the HCFs with Kagomé claddings do not possess photonic band gaps in the form that exists in photonic-crystal HCFs. All dispersion dependences of the cladding modes are distributed quite uniformly over the entire transmission spectrum of the HCF with a Kagomé cladding (see Fig. 2). According to the ideas presented in Ref. [21], the suppression of coupling between the modes of the air-core and those of the Kagomé cladding occurs due to the strong mismatch between the transverse distributions of the fields of these modes. The cladding modes arising in the bridges of the Kagomé cladding have a strongly oscillating spatial structure, so that the integrals of their overlap with the air-core modes are very small. Hence, the Kagomé HCFs ensure transmission in much wider spectral intervals than photonic-crystal HCFs do (see Fig. 1). As an example, we can consider the HCF with Kagomé cladding from Ref. [22], in which the radiation propagated with losses of less than 1.5 dB m^{-1} in the interval of wavelengths from 600 to 800 nm. Nevertheless, although these losses are low enough for some applications, they strongly increase with growing wavelength. Therefore, HCFs with Kagomé cladding made of fused silica cannot be used to transmit radiation in the mid-IR spectral range.

When speaking of HCFs with microstructured cladding aimed at transmitting radiation in the mid-IR spectral region, it is impossible to ignore Bragg hollow-core fibers [23]. In this case, it is common to say that the cladding of such an HCF is a one-dimensional photonic crystal. The periodically arranged layers of the cladding with different values of the refractive index form a Bragg mirror that efficiently reflects the radiation traveling along the air-core and thus forming a guided mode (Fig. 3). In Ref. [23], the layers consisted of glass with high refractive index and layers of a polymer with a lower refractive index. According to the measurements, such an HCF could transmit radiation from 0.75 to 10.6 μm, depending on the thickness of the cladding layers. At a wavelength of 10.6 μm, the losses of the Bragg HCF amounted to < 1 dB m^{-1}. Nevertheless, the transmission of high-power radiation in such HCFs is likely to be impossible, because, since the publication of this paper, there have been no reports of increasing the power of transmitted radiation in the mid-IR range.

The ideal resolution of this situation would be to make such HCFs from fused silica that have a relatively simple cladding structure and could be thought to both lower losses in the telecommunication spectral region (~ 1.55 μm) and transmit high-power radiation in the near IR and mid-IR ranges. Such HCFs with a curved shape of the core boundary appeared in 2011 at the Dianov Fiber Optics Research Center of the Russian Academy of Sciences [2] and were called revolver HCFs. The research team of Prof. Benabid reported a similar effect in the case of localization of radiation in the air-core of an HCF with Kagomé cladding and a curved core boundary [3] (Fig. 4c).

At the same time, in Ref. [2] it was demonstrated that, despite high material losses of fused silica and a relatively simple structure of the HCF cladding (Fig. 4a), the radiation could be transmitted with low losses in the mid-IR range up to a wavelength of 4 μm, in contrast to photonic-crystal HCFs and HCFs with Kagomé cladding. Later, a construction of a revolver HCF was proposed, in which the capillaries of the cladding were not in contact with each other [4] (Fig. 4b), which weakened the coupling between them and allowed transmitting radiation in more longwave regions of the mid-IR range. In the case of Ref. [3], the spectrum of transmission with relatively low losses was restricted to the near-IR range. Subsequently, new [24] and modified [25–27] fused silica HCF constructions with a curved boundary of the core were proposed (Fig. 5), experiments with which confirmed that such HCFs localize radiation with low losses in the air-filled core and, what is most important, the air-core modes very

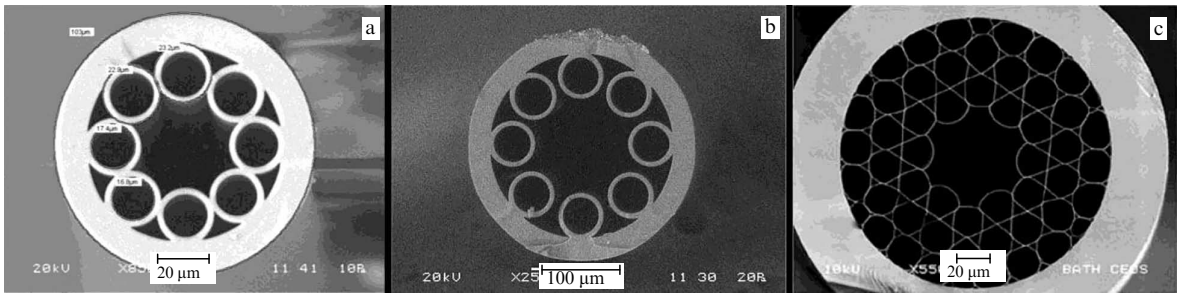

Figure 4. (a) Cross section of a fused silica HCF with a curved core boundary. (Adopted from Ref. [2].) (b) Cross section of a fused silica HCF with a curved core boundary and separated capillaries of the cladding. (Adopted from Ref. [4].) (c) Cross section of a fused silica HCF with a Kagomé cladding and curved core boundary. (Adopted from Ref. [3].)

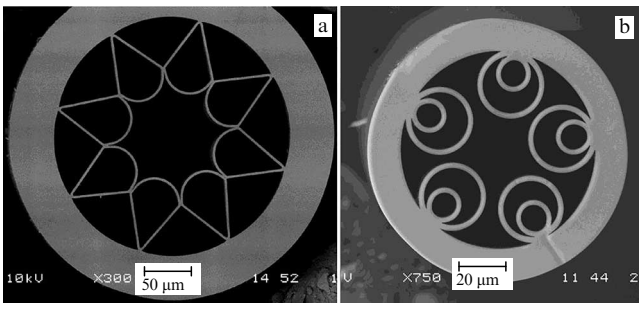

Figure 5. (a) Cross section of a fused silica HCF with a curved core boundary (Adopted from Ref. [24].) (b) Cross section of a fused silica nested hollow-core fiber allowing significant loss reduction. (Adopted from Ref. [26].)

weakly overlap with the HCF cladding. It was exactly the last factor that was the determining one for the transmission of radiation with low losses in a fused silica HCF wit a curved boundary of the core in the mid-IR range.

One of the main questions that arises when considering HCFs with a curved core boundary is the understanding and formulation of light localization in the air-core making it possible to obtain the above results. Clearly, in this case, there is no two-dimensional photonic crystal in the HCF cladding with the appropriate translation symmetry. Therefore, it is impossible to explain the localization of radiation in such HCFs by the presence of a PBG. On the other hand, some authors [28] approached explaining the radiation localization in HCFs with a curved core boundary based on the same ideas as the explanation of localization in HCFs with Kagomé cladding [21]. This approach, as mentioned above, is based on minimizing the value of the overlap integral between the air-core mode and the modes of the HCF cladding and is referred to as the inhibited coupling model. Historically, this was because the first HCFs of the research team trying to substantiate light localization in an HCF with a curved boundary using this model were those with Kagomé cladding (Fig. 4c). That is why the authors of Ref. [28] automatically transferred the abovementioned model to the new type of HCF.

At the same time, the most common point of view on the mechanism of radiation localization in an HCF with a curved core boundary is the phenomenon of anti-resonance, also described above. The approach considered in the first studies of this issue [12] has been generalized to the case of not only planar optical waveguides but also all microstructured optical fibers, including HCFs [29], and was called the antiresonant optical waveguide (ARROW) model. The meaning of this model in general terms is that any HCF cladding element having a finite thickness t can be considered a Fabry–Perot microresonator at a given wavelength λ. Then, the wavelengths corresponding to the minimum losses of the transmission bands of the HCF are determined by the formula

$$\frac{2\pi t}{\lambda}\sqrt{n^2-1}=\left(m+\frac{1}{2}\right)\pi\,, \tag{1}$$

where n is the glass refractive index, $m=0,1,2,\ldots$.

The wavelengths corresponding to the maximum losses in the HCF transmission spectrum will be determined as

$$\frac{2\pi t}{\lambda}\sqrt{n^2-1}=m\pi\,. \tag{2}$$

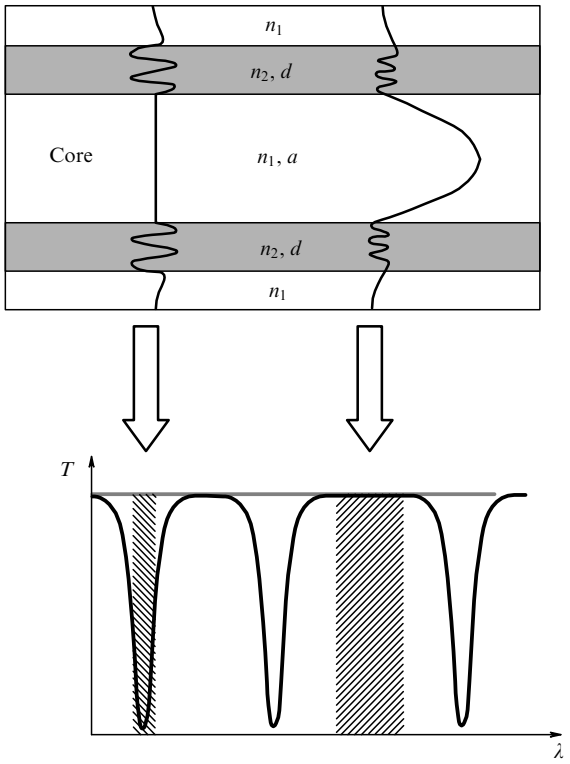

Figure 6. Anti-resonant model for a planar waveguide with wall thickness d and core size a; n_1 and n_2 are refractive indices (top), transmission bands of waveguides are shown in the bottom figure (T is the waveguide transmission coefficient). (Adopted from Ref. [29].)

The ARROW model is shown schematically in Fig. 6.

Whereas the positions of the HCF transmission band edges are described by Eqn (2) with fairly good accuracy, the explanation of the degree of localization of radiation in the air-core that allows light transmission through an HCF with a curved core boundary at huge material losses in the cladding cannot simply be described by approximation (1) for planar waveguides. The main drawback of the ARROW model as applied to HCFs with a curved boundary of the core is that it ignores the shape of this boundary.

For a deeper understanding of the mechanisms of light localization in an HCF with a curved core boundary, it is possible to consider such a quantity to be the local velocity of the core mode energy flow at the core boundary. It is a function of the transverse coordinates only [30]:

$$\mathbf{V}(r,\varphi)=\frac{\mathbf{P}}{W}\,, \tag{3}$$

where $\mathbf{P}=(1/2)\,\mathrm{Re}\,(\mathbf{E}\times\mathbf{H}^*)$ is the Poynting vector of the HCF air-core mode, $W=(1/4)(\varepsilon|\mathbf{E}|^2+\mu|\mathbf{H}|^2)$ is the energy density of this mode, and (r,φ) are the coordinates of a point in the HCF cross section.

Let us consider two HCFs with similar diameters of air-filled cores and similar thicknesses of the cladding elements. Let one of them be an individual capillary of fused silica with a core diameter of 50 μm and wall thickness of 750 nm (Fig. 7a), and the other a fused silica HCF with the cladding made of eight capillaries (Fig. 7b) and similar geometrical parameters. Let us calculate the distribution $V_r(r,\varphi)$ of the radial projection of the local energy velocity at a wavelength of 1.06 μm for the fundamental mode of the air-core along the inner boundary of an individual capillary and along the outer

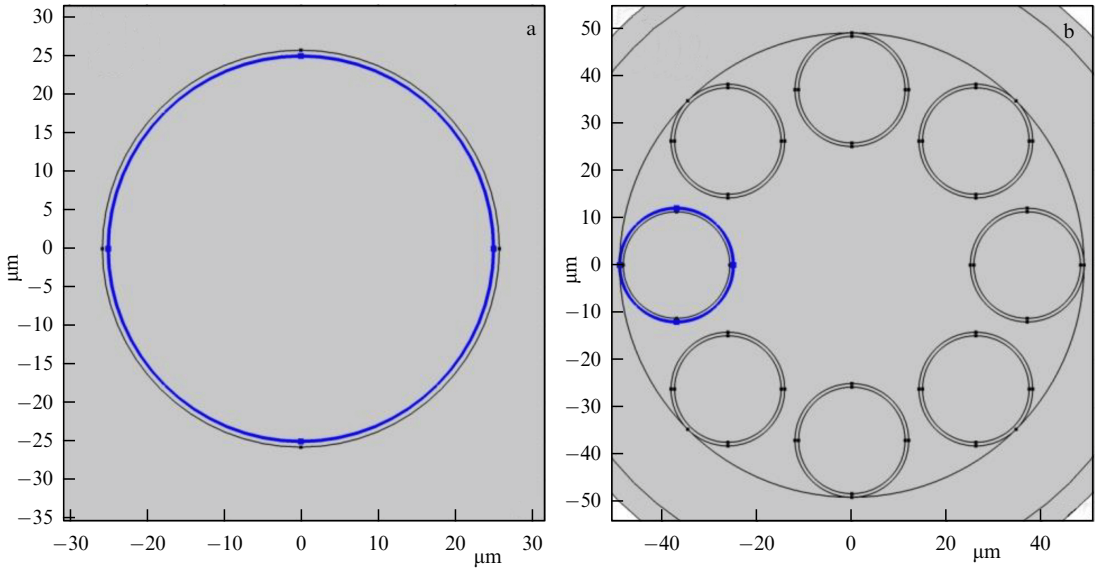

Figure 7. (a) Inner boundary of a capillary; (b) outer boundary of an individual capillary of the HCF cladding. (Adopted from Ref. [30].)

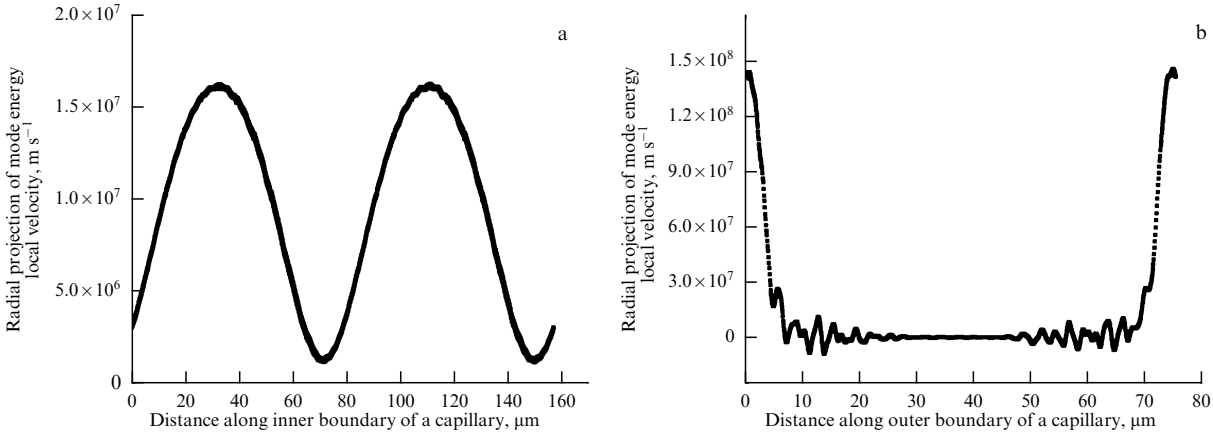

Figure 8. (a) Distribution $V_r(r, \varphi)$ for the fundamental mode of the core along the inner boundary of a capillary (Fig. 7a); (b) distribution $V_r(r, \varphi)$ for the fundamental mode along the outer boundary of an individual capillary of the HCF cladding (Fig. 7b). (Adopted from Ref. [30].)

boundary of the HCF cladding capillary (see Fig. 7). This is necessary in order to understand the difference between the energy leakage of the air-core mode along the internal boundaries of an individual capillary as a waveguide, for which the ARROW model is valid, and that along the curved boundary of the HCF.

The corresponding distributions $V_r(r, \varphi)$ for the fundamental air-core mode of the hollow core are shown in Fig. 8.

It is obvious that in an individual capillary the radial projection of the local velocity of the energy of the air-core fundamental mode nowhere becomes zero and nowhere takes negative values (Fig. 8a). At the same time, the radial projection of the energy local velocity of the air-core fundamental mode along the outer boundary of an individual capillary of the HCF cladding behaves in an oscillatory manner and has zero and negative values in many areas (Fig. 8b). It takes the maximum positive value at the point of the capillary attachment to the basic tube. This indicates a significantly more complex nature of the interaction between the radiation of the air-core mode and the curved core boundary, which is very different from that described by the ARROW model. Naturally, this difference leads to a difference in the losses for the two optical fibers shown in Fig. 8. For the capillary (Fig. 8a), the losses were 12 dB m^{-1}, whereas for the HCF (Fig. 8b), they amounted to 1.2 dB km^{-1}. Such a difference in the interaction of radiation between two hollow-core optical waveguides is explained by the formation of complex vortex motions of the power flux of the fundamental mode of the hollow core in the walls of capillaries of the HCF cladding (Fig. 7b) arising due to the presence of singularities in the transverse component of its Poynting vector [31].

1.2 Technology of fabricating hollow-core optical fibers

1.2.1 Fabricating hollow-core optical fibers from fused silica

The main method of making practically all glass optical fibers, including microstructured ones, is the drawing of the fiber from a macroscopic preform. The preform already has a structure (one or several cores, reflective claddings, stressing rods, etc.) that is inherited by the drawn fiber. The preforms can be fabricated using different methods, the most widespread one for microstructured fibers being the 'stack and draw technique.' Figure 9 shows the stages of applying the stack and draw technique to fabricate a microstructured

optical fiber, namely, a revolver hollow-core fiber with nested capillaries.

Initially starting from the design of the HCF to be produced and considering the method of fiber drawing, the structure of the preform is designed and the dimensions of all preform elements are calculated (Fig. 9a). Then, the elements of HCF cladding are made of silica tubes. For this purpose, the tubes are inserted one into another and fused together using oxygen-hydrogen burner. The resulting structure is drawn on a standard drawing tower, thus making the constituents of the composed preform (Fig. 9b). In a similar way, the support elements are drawn on a standard drawing tower (Fig. 9c). Then all prepared elements are sorted to choose the necessary number of elements with minimum deviations from the required dimensions. At the next stage the stacking of the preform is carried out. The auxiliary elements are used at the preform edges to position the main elements correctly (Fig. 9d). After that, the stacked preform is processed on a glassblowing lathe in such a way that structural elements would be fused into the desired configuration without substantial deformation. Then, cane drawing is performed (Fig. 9e). Finally, the fiber is drawn with simultaneous jacketing with a thick-wall tube (Fig. 9f). In the process of drawing, excessive gas pressure is supported in the preform cavity, which allows reducing the structure deformation under the action of surface tension forces. Usually, gas pressure regulators are used for this purpose, which are connected to all cavities in the preform and support the necessary extra pressure. There is also an alternative approach to the pressure regulation in the preform, called 'the technology of drawing with a sealed upper end' [32]. The essence of the technology is that the cavities of the preform are sealed from the upper end and the pressure is increased in the process of drawing due to the preform heating. The advantage of this method is that all cavities are enlarged by the same number of times, regardless of their initial size. Thus, this technology allows producing optical fibers with many various cavities without using high-precision gas pressure regulators.

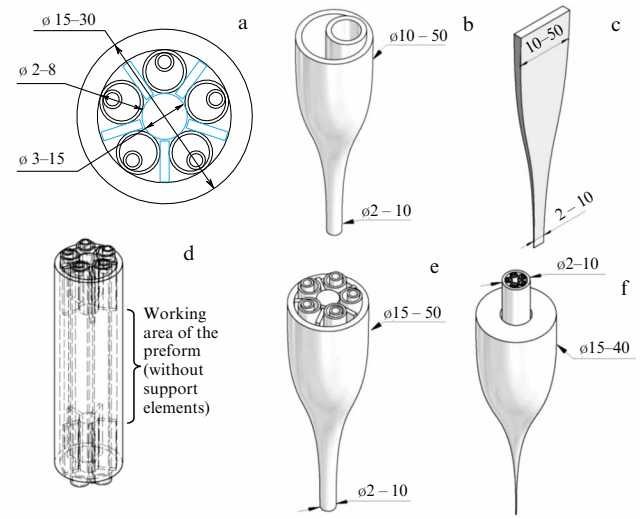

Figure 9. Stages of fabricating a hollow-core revolver fiber with nested capillaries (typical dimensions of elements given in millimeters): (a) preform cross-section drawing (support elements shown in blue); (b) draw composite elements with nested capillaries; (c) draw auxiliary elements; (d) assembled preform; (e) draw to fiber cane; (f) draw down to final fiber.

In addition to the above technology for fabricating microstructured optical fibers, the extrusion method [33] is successfully used for low-melting glass, which consists of pressing softened glass through special dies with a complex shape.

Recently, a method of 3D printing of the preforms is also under active development [34]. The main advantage of this method is the possibility of obtaining preforms of arbitrarily complex shapes. It is important to note that the improved 3D printing method allows fabricating not only plastic but also glass optical fibers [35, 36]. In this technology, a fine-dispersed glass powder (up to 70 wt%) is admixed to the polymer. After the print, the preform is subjected to annealing, in the process of which the organic compounds are burned out and the porous carcass of glass is left. This material can be sintered, which yields a glass product of optical quality with the conservation of the structure determined by the printing.

1.2.2 Prospects and soft glasses. Although the dominant part of the radiation in HCFs is localized in the core, HCFs of fused silica demonstrate high optical losses in the mid-IR range because of high absorption by silica in this region (more than 1000 dB m^{-1} for wavelengths above 4 μm) [4]. Although there are reports of silica HCFs operating in the mid-IR range [37–39], such fibers are inapplicable in the wavelength range above 4.5 μm [24]. Obviously, the transition to longer wavelengths requires the abandonment of fused silica, despite all the advantages of this material, namely its high manufacturability, mechanical strength, and low optical losses.

First of all, fluoride, tellurite, and chalcogenide glasses should be considered promising materials for the production of mid-IR range HCFs.

Fluoride glasses. ZBLAN is the most well-known and manufacturable fluoride glass. This is a group of glasses with the $ZrF_4-BaF_2-LaF_3-AlF_3-NaF$ composition developed in 1974 [40]. ZBLAN glasses are being actively introduced into the fiber optics of the mid-IR range. The region of optical transparency of ZBLAN glasses ranges to 7 μm. Fabricating hollow-core fibers of this glass could allow considerable extension of the application field of hollow-core optical fibers. However, this class of glasses has significant disadvantages, the main one being the strong hygroscopicity of the surface, due to which even standard all-glass ZBLAN fibers require special protection of the end faces from atmospheric air. The development of ZBLAN hollow-core optical fibers must take this material feature into account from the very beginning. In other words, it is necessary to provide reliable protection of all surfaces at all stages of production and operation of ZBLAN hollow-core fibers.

The second significant disadvantage of the considered glasses is the strong temperature dependence of the material viscosity, which substantially complicates the production of microstructured optical fibers. Nevertheless, it is possible to fabricate microstructured optical fibers of this glass [41, 42]. However, in the literature, we could not find experimental papers on the successful fabrication of hollow-core fibers of fluoride glasses. We can only mention theoretical paper [43], in which the structure of a hollow-core ZBLAN glass fiber is proposed. Thus, the development and creation of hollow-core fibers based on heavy metal fluorides is a very challenge.

Chalcogenide glasses. The term 'chalcogenide materials' refers to a large class of materials containing one or more chalcogens other than oxygen. In other words, chalcogenide materials and chalcogenide glasses are contrasted with oxide glasses and materials. Depending on the composition of the glass, the range of optical transparency can be from 1 to 20 μm. Many chalcogenides vitrify well, and therefore they can be used for the fabrication of optical fibers. The most popular chalcogenide glasses that are successfully used in fiber optics are glasses of As–S systems: As–Se, Ge–As–S, Ge–As–Se–Te, etc. The first hollow-core optical fiber made of chalcogenide glass was fabricated in 2010 [44]; $Te_{20}As_{30}Se_{50}$ glass was used, and the optical fiber had a multilayer reflective cladding. The fiber preform was made by stack and draw technique and consisted of six rows of capillaries stacked from 162 elements. Two samples of hollow-core fibers with a core diameter of 32 and 58 μm were drawn from the preform, the first layer of glass delimiting the core was very thick, and the shape of the core–cladding boundary was close to round. Unfortunately, the authors were unable to observe the light propagation through the hollow core of fabricated samples in the range of 2–20 μm. But already the following year, a hollow-core optical fiber with a revolver structure was demonstrated, also made of glass with the composition $Te_{20}As_{30}Se_{50}$; the fiber cladding consisted of eight contacting capillaries, the optical fiber was made by stack and draw technique, the core diameter was 380 μm, and the thickness of the capillary wall was 13 μm. The transmission of CO_2 laser radiation through the hollow core of this optical fiber was demonstrated for the first time. The optical loss in this fiber was 11 dB m^{-1}. Also, chalcogenide glasses can be formed by extrusion; for example, in [45], a revolver-type hollow-core chalcogenide fiber was used for spectroscopy in the mid-IR range. This fiber was produced by extrusion and showed an optical loss of 0.1 dB m^{-1} at a wavelength of 10.5 μm.

Features of chalcogenide glasses include a strong dependence of viscosity on temperature (this is a common problem with all low-melting glasses). A significant problem with chalcogenide glasses is the heterogeneity of the composition, since all glasses of this class allow a wide range of component concentrations; when forming bulk glass samples, the glass often segregates into domains with different compositions. This, in turn, leads to viscosity inhomogeneities, which makes the fabrication of microstructured optical fibers very difficult. Also, one should not forget about such problems of chalcogenide glasses as the toxicity of components and low strength of glass compared to silicate glasses.

Tellurite glasses. Tellurite glasses are those based on tellurium oxide. Unfortunately, pure tellurium oxide is very prone to crystallization, and additives of other oxides are used to stabilize the glass. In relation to fiber optics, two systems are most widely used: zinc-tellurite and tungstate-tellurite glasses [46]. The glass transparency range of both systems extends to 5 μm. Compared to chalcogenide glasses, tellurite glass is less toxic and more technologically advanced. The main problem with tellurite glasses is the admixture of OH groups, which is extremely difficult to get rid of; even a small content of OH groups in the glass leads to significant losses in the range of about 3 μm. Nevertheless, researchers can dehydrate tellurite glasses to very high purity [47]. Tellurite glasses are actively used to create microstructured optical fibers, including hollow-core ones. For example, Ventura et al. [48] demonstrated a tellurite HCF for transmitting single-mode laser radiation with a wavelength from 4.9 to 6 μm, and Ref. [49] reported delivering mid-infrared radiation at a wavelength of up to 10 μm with a low loss of 2.1 dB m^{-1}.

2. Revolver optical fiber as the basis of promising optical communication lines

Hollow-core optical fibers open new prospects in the area of fiber-optic communication lines, since the abandonment of the solid-state core will also remove the fundamental limitations imposed by the core material on the optical characteristics of optical fibers. For transmitting information over long distances, the key characteristic of fibers is the amount of optical loss.

In modern telecommunication fibers, optical losses have a minimum at a wavelength of 1.55 μm, which is ~ 0.15 dB km^{-1} and has already been reached in practice. The spectral position and magnitude of the minimum optical loss is determined by mechanisms such as Rayleigh scattering and phonon absorption in fused silica. However, when moving to hollow-core fibers, in most cases filled with air, the concentration of molecules in the core drops by more than three orders of magnitude, which radically reduces the influence of scattering and absorption processes in the core on optical losses. The ability to pump air out of the core further raises the question of how much optical loss can be reduced in hollow-core fibers compared to modern telecommunications fibers. In addition, the hollow core can provide a wide spectral bandwidth and transmit information at the speed of light in a vacuum, which is ~ 1.5 times faster than silica core fibers. Another advantage is the strong suppression in the hollow core of unwanted nonlinear effects that create noise in communication lines. Taken together, these advantages of hollow-core fibers create prospects for significantly increasing the capacity of next-generation fiber-optic communication lines.

The desire to outperform modern telecommunications fibers and reduce the minimum optical loss below the fundamental limit (~ 0.15 dB km^{-1}) has stimulated active research on hollow-core fibers since their inception [1]. It quickly became clear [18] that photonic-crystal type hollow-core fibers, which were the first to appear, do not allow solving this problem. The minimum level of optical loss demonstrated in such fibers is ~ 1.2 dB km^{-1} at a wavelength of 1620 nm. In this case, the limiting factor is the scattering of radiation at the roughness of numerous air–glass interfaces in a microstructured cladding.

Although the amplitude of roughness at air–glass interfaces is very small (less than 1 nm), it cannot be completely eliminated [18]. Therefore, to reduce optical scattering losses, it was necessary to reduce the proportion of radiation interacting with the interface between the hollow core and the microstructured cladding of the fiber. This was reached with the advent of antiresonant hollow-core fibers with negative curvature of the core–cladding interface [2, 4, 37, 50]. Such fibers not only renewed the hope for overcoming the fundamental limit of optical loss in telecommunication fibers but also showed the possibility of reaching low optical loss over a wide spectral bandwidth (Fig. 10). In this case, a particularly important role was played by the revolver-type hollow-core fibers developed at the Fiber Optics Research Center of the Russian Academy of Sciences [2, 4], which significantly simplified the design and fabricating technology of hollow-core fibers and, thus, served as a starting point for

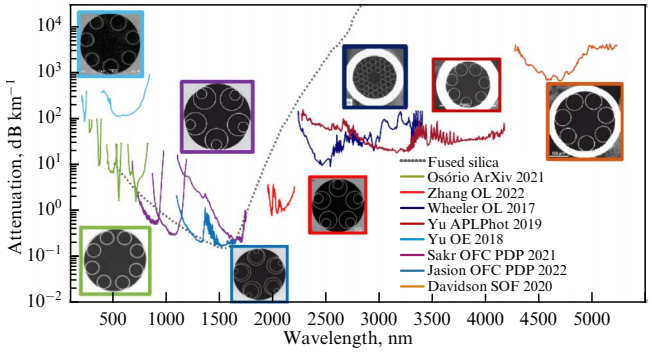

Figure 10. Optical losses demonstrated in antiresonant hollow-core fibers. From left to right: (blue) Yu et al [54]; (green) Osório et al. [55]; (violet) Sakr et al. [63]; (blue) Jasion et al. [53]; (red) Zhang et al. [56]; (dark blue) Wheeler et al. [57]; (dark red) Yu et al. [58]; (orange) Davidson et al. [59]. For comparison, dotted line shows optical losses in bulk fused silica.

the further development of new types of hollow-core fibers [25, 26, 51–53].

In revolver-type hollow-core fibers, the main contribution to optical losses comes from the leakage of radiation from the hollow core into the fiber cladding. To suppress this mechanism of optical loss, the most productive approach turns out to be the use of nested capillaries in the fiber cladding [25, 26]. Subsequently, it was HCF with nested capillaries that became the main type of hollow fiber considered for telecommunication applications. Already in 2014, using numerical modeling methods, it was shown that the leakage losses of the fundamental mode in such fibers can be as low as 0.1 dB km^{-1} at wavelengths from 1.5 to 2.5 μm [26]. This result gave new impetus to active research on the optical properties and improvement of the technology for fabricating such fibers.

Over the past five years, optical losses in hollow-core fibers have decreased at an impressive rate. Researchers from the University of Southampton have experimentally demonstrated hollow-core fibers with optical losses of 1.3 dB km^{-1} (2018) [60] and 0.65 dB km^{-1} (2019) [61]. Optimizing the technology for drawing long (more than 1 km) sections of hollow-core fibers with nested capillaries, as well as improving measurement techniques, allowed the same group to reduce optical losses to 0.28 dB km^{-1} (2020) [62]. And the optimization of the optical fiber cross-section geometry led to a reduction in losses, first to 0.22 dB km^{-1} (2021) [63], and then to a record low value of 0.174 dB km^{-1} (2022), reached using double-nested capillaries in the optical fiber cladding [53].

Thus, today, hollow-core fibers have already reached a level of optical loss comparable to the fundamental limit of modern telecommunication fibers in the spectral region of about 1.55 μm. Moreover, numerical simulation results indicate that optical loss as low as 0.055 dB km^{-1} [5] can be reached in hollow-core fibers with double-nested capillaries.

The practical implementation of such low optical losses will open a fundamentally new page in the field of fiber-optical communication lines. Today, various scientific groups and telecommunication companies are experimenting with data transmission through hollow-core fibers [64–68].

The current level of technological development makes it possible to produce hollow-core optical fibers several kilometers long, as well as to splice them, and the optical losses introduced by the spliced connection of hollow-core optical fibers amount to a rather small value of ~ 0.2 dB [66, 68]. Thus, one of the first practical applications of hollow-core fibers may be the transmission of information over short distances ($\leqslant 10$ km) inside data centers or financial organizations, for which it is critical to receive up-to-date information with minimum time delays. Laboratory experiments [64, 65] demonstrated the possibility of transmitting data through a ~ 1-km-long hollow-core fiber. At the same time, the information transmission rate was 100 Gb s^{-1} per spectral channel. It should be noted that the total data transfer rate can easily be scaled, given the exceptionally wide (~ 700 nm) bandwidth of the hollow-core fiber used in the experiments.

An increase in the information transmission distance in hollow-core fibers with nested capillaries up to hundreds of kilometers in length was demonstrated in Ref. [66]. Two fibers with lengths of 3.4 and 4.3 km were spliced into one segment 7.7 km long, which was closed in a loop for repeated recirculation of the optical signal. Using a symbol rate of 32 Gbaud and trying various modulation formats, a data transmission range of ~ 618 km was reached.

The transition from laboratory experiments to deployment of communication lines under real field conditions requires the creation of a fiber-optic cable based on hollow-core optical fibers. The technology of laying an optical fiber in a cable is an important component in real communication networks, since the optical fiber in a cable can be subject to micro- and macrobending, increasing optical losses in the communication line. Recent paper [68] demonstrated a fiber optic cable based on a hollow-core optical fiber with double nested capillaries, which reached a data transmission range of more than 1000 km in a 48-channel wavelength division multiplex link with a transmission rate of 800 Gbit s^{-1} in each channel.

Thus, the potential capabilities of hollow-core optical fibers are being systematically realized, and hollow-core fibers themselves are increasingly becoming a realistic basis for the next generation of high-speed fiber-optic communication lines.

3. Transporting radiation with high mean and/or peak power

3.1 Properties of standard and hollow-core optical fibers: a comparison

As the power of laser radiation propagating along an optical fiber of any type increases, starting from a certain threshold power value, radiation-induced damage to the optical fiber may occur.

In the most obvious cases, damage to the fiber occurs because of a thermal micro-explosion: in a certain small volume of the fiber material, the energy release exceeds the amount of heat that is removed due to thermal conductivity. The flux of heat removed due to thermal conductivity increases approximately in proportion to the temperature. If heat generation increases faster with temperature, then the conditions for a thermal explosion are realized. In this case, heating the substance above the temperature of parity between heat release and thermal conductivity losses leads to further heating, which accompanies an increase in the absorption coefficient of light radiation; as a result, the heating rate of the substance increases. This avalanche-like process is the above microexplosion. As a simple example, let us consider the possibility of destructing a silica standard

communication fiber (with a solid glass rather than hollow core) due to heating by laser radiation. Its optical loss is about 0.2 dB km^{-1} (at a wavelength of minimum loss) at room temperature and increases drastically at a temperature of the order of $T_l \sim 1100\,^{\circ}C$ [69]. If we assume for estimation that the optical losses in the fiber are due only to the absorption of radiation (which obviously overestimates the heat energy release), then we can estimate the threshold power of laser radiation, above which a thermal explosion develops (from the condition of equality of energy release in the core and heat removal from the core due to thermal conductivity) in the following form:

$$P_{th} = \frac{2\pi T_l \lambda_T}{\alpha},$$

where $\lambda_T = 1.46$ W (m °C)$^{-1}$ is the thermal conductivity coefficient of fused silica, and $\alpha = 0.2$ dB km^{-1} (4.6×10^{-5} m^{-1}) is fiber optical losses. The threshold power P_{th} under the assumptions made turns out to have a relatively high value of $P_{th} \approx 200$ MW.

There are also other processes that can limit the power of radiation transmitted through an optical fiber, which are characterized by significantly lower threshold power values. When the light radiation of sufficient intensity propagates through the core of a fused silica fiber (again, for simplicity, we consider a fiber with a solid core), a nonlinear process such as stimulated Raman scattering (SRS) develops, i.e., the conversion of pump radiation quanta into quanta of lower energy (the Stokes frequency shift) leading to a significantly greater thermal effect (compared to the example discussed above). As was shown by Biriukov et al. [70], when single-mode radiation propagates through a fiber with a core diameter of 8 μm, the threshold power value is $P_{th} \sim 10$ kW. This estimate agrees with available experimental data: single mode CW fiber lasers have an output power not exceeding several kilowatts. In the absence of thermal equilibrium when transmitting short radiation pulses, the threshold value of the peak pulse power turns out to be significantly higher than the values characterizing CW radiation. Currently, special solid-state silica fibers have demonstrated the generation of laser pulses with a peak power reaching ~ 1 MW [71]. Another process that limits the maximum power transmitted through a silica-core fiber is self-focusing. The threshold power for self-focusing in fused silica is of the order of 1 MW [72] and is thus comparable to the experimental values reached.

In contrast to all-solid-state optical fibers based on fused silica, hollow-core optical fibers, also made of fused silica, are more resistant to high transmitted radiation powers, even though heat removal from the field-confining elements in the hollow core is more difficult than with all-solid-state optical fibers. This resistance is primarily due to such a distribution of the radiation field in the HCF that almost all the power is transmitted through the hollow core, usually filled with gas, and the power propagating through the glass elements of the reflective cladding is $\sim 10^{-5}$ of the total power. In addition, the hollow core of an optical fiber is usually filled with air, the density of which is three orders of magnitude lower than the density of a solid, because of which nonlinearity coefficients of the gas as an optical medium are also approximately three orders of magnitude lower. Recently, it was shown possible to transport radiation with a power of 1 kW over 1 km along an HCF with a core diameter of 31 μm [73] and CW narrow-band (84 GHz) radiation with a power of 2.2 kW over a distance of about 10 m along an HCF with a core diameter of 23 μm [74]. This is a direct demonstration of the unique capabilities of HCFs for transporting high-power laser radiation due to their exceptionally low nonlinearity and high destruction thresholds. The core of the HCF is usually filled with air; the threshold self-focusing power in air at atmospheric pressure is also about three orders of magnitude higher than in most solid-state optical materials and amounts to ~ 3 GW [75]. This value also limits the maximum possible power that can be transmitted through an HCF (without additional core vacuumization). And, relatively recently, the transmission of pulses (hundreds of femtoseconds long) with such a peak power was experimentally realized using a revolver-type fiber [76], that is, with a peak power approximately three orders of magnitude higher than the maximum values for all-solid-state fibers.

It should be noted that, when most of the radiation propagates through a narrow hollow core filled with air, it is necessary to consider the possibility of optical breakdown of the air under the effect of laser radiation. Optical gas breakdown has been widely studied, especially at the beginning of the laser era, and the available data show that the threshold laser light intensity for breakdown in atmospheric-pressure air is of the order of 10^{11} W cm^{-2} for nanosecond pulses, increasing to $\sim 10^{14}$ W cm^{-2} for shorter pulses with a duration in the picosecond range [77]. The threshold power varies depending on the diameter of the focusing area (in the case of hollow-core fibers — on the diameter of the hollow core) approximately as $\sim d_c^{-3/2}$. Apparently, this explains the fact that, in numerous experiments carried out by the authors, in which the laser radiation with an intensity of $\sim 10^{12}$ W cm^{-2} propagated along a hollow-core fiber, no spontaneous optical breakdown in the core was observed [78]. Thus, the ability of the HCF to transport pulsed laser radiation with approximately three orders of magnitude higher power than all-solid optical fibers (with a fused silica core) is demonstrated.

Observing the actual process of destruction of an optical fiber under the action of high-power laser radiation faces great experimental difficulties, since the point of destruction occurrence is usually not localized; it is determined by the random distribution of sites of relative weakness in the structure of the fiber under study. In addition, such experiments require the use of high-power lasers, which increases the cost of these experiments. But another approach to studying this problem is also possible. The fact is that, after the formation of a strongly radiation-absorbing region in the optical fiber (plasma), this region, under the influence of the same laser radiation, begins to move towards the laser, destroying the optical fiber — the so-called fiber fuse effect [79] takes place. Since the phenomenon of plasma formation under the influence of an electromagnetic field is usually called discharge [80], we can say that, in this case, we are dealing with the propagation of an optical discharge along an optical fiber. And the speed of such propagation can range from meters per second to kilometers per second, depending on the intensity of the laser radiation [81, 82].

It is obvious that the propagation of an optical discharge along optical fibers has much more catastrophic consequences for fiber systems than does destruction at one point during, e.g., a 'pure' thermal explosion. And, second, the phenomenon of optical discharge propagation has significantly lower threshold conditions for radiation power than a thermal explosion. When these threshold conditions are exceeded, the optical fiber finds itself in a kind of unstable

state, namely, if a plasma source is accidentally formed in some way in the energy transport channel, the radiation-supported plasma begins to move towards the laser radiation, destroying the optical fiber.

A fiber line in which the laser radiation intensity is below the threshold for the propagation of an optical discharge is much safer. In solid-state fibers based on fused silica with a not small mode field diameter (more than 8 μm), an intensity of laser radiation of the order of 1 MW cm^{-2} is sufficient for the propagation of an optical discharge, which corresponds to a total transmitted radiation power of only a few watts. A report on the results of studying this process can be found in Refs [82, 83]. As to the possibility of a similar effect in hollow-core fibers, only a few years ago such an effect was observed in an HCF [78, 84, 85]. Since, in fact, the conditions of supporting the optical discharge propagation along the optical fiber determine the possibility of its application under 'nonsterile' real exploitation conditions, we will dwell on these results in more detail.

3.2 Propagation of optical discharge through a revolver optical fiber

Usually, the simplest picture of interaction between laser radiation and a fiber core in the process of destructive wave propagation along the fiber is observed when CW laser radiation is used [69, 70, 86]. However, to date, it has been impossible to observe the destruction wave propagation along an HCF under such conditions. Apparently, this fact is explained by the necessity to use CW lasers of sufficiently high power in experiments. Some idea of the physical processes that can take place during HCF destruction under exposure to CW laser radiation can be obtained using the results of Ref. [87]. In this paper, the processes of propagation of air plasma supported by laser radiation (i.e., optical discharge (OD)) were also studied in glass tubes (as in HCFs), but of much greater diameter, of the order of 10 mm (for comparison, the HCF hollow-core diameter is commonly a few ten up to a hundred micrometers). The experiments were carried out in a quasicontinuous regime, since the duration of the laser pulses ($\lambda = 1.06$ μm) amounted to about 5 ms, which exceeded all characteristic times of the process studied. From the results of Ref. [87], it follows that, when a center of laser radiation absorption arises inside the tube, an optical discharge develops there, which travels along the tube towards the laser at a relatively low intensity of the quasi-CW laser radiation (~ 1 MW cm^{-2}, the laser power being about 2 MW). As the laser radiation intensity increases, the regime of OD propagation changes from thermal conduction to optical detonation (see [80]). In this case, the observed velocity of OD propagation increases from nearly 1 m s^{-1} to 2 km s^{-1}. Similar processes are expected to occur in HCFs, with a correction for the substantially smaller diameter of the core.

The value of laser radiation power required for the propagation of CW OD along a hollow-core optical fiber can be estimated in the following way. It is known that the threshold intensity of laser radiation for the propagation of an OD along a tube depends on the tube diameter as $I_{th} \sim 1/d_c$ [80]. Such a dependence on the tube diameter appears due to the energy losses along the radius to the tube walls. Therefore, based on the data of Ref. [87], we conclude that, for an HCF with a core diameter of 20 μm, the threshold power should be of the order of 500 W (the laser radiation intensity in the fiber being $I_{th} \sim 5 \times 10^8$ W cm^{-2}).

When using lasers with lower average power, observation of the formation and propagation of plasma along the HCF is also possible, but in pulse-periodic regimes, which provide significantly higher radiation intensities in the fiber core than the above estimate for CW radiation. Thus, when 10-ns pulses of Nd:YAG laser radiation propagated through a photonic-crystal optical fiber with a hollow core filled with atmospheric air, a limitation on the energy of pulses transmitted along an 8-mm-long optical fiber was observed due to the occurrence of optical breakdown at a laser radiation intensity of about 6.2×10^{11} W cm^{-2} [88]. In another paper [89], when transporting nanosecond pulses (Nd:YAG, $\tau = 12$ ns, frequency of 10 Hz) through an HCF (Kagomé fiber, core diameter of 50 μm), spontaneous initiation of the fiber destruction process was observed in several experiments at radiation intensities of about 5×10^{10} W cm^{-2} in the core, after which a destruction wave propagated along the optical fiber towards the laser with an average velocity of ~ 5 cm s^{-1}. In this case, the reflective microstructured cladding of the optical fiber was completely destroyed. When proceeding to ultrashort pulses, the threshold intensities of HCF destruction increase. Thus, in Ref. [90], the possibility of delivering femtosecond (duration of ~ 100 fs) pulses with an intensity of up to 10^{11} W cm^{-2} through an HCF (a revolver optical fiber was used as the HCF) over a distance of 10 m without degradation of radiation parameters was shown. In this case, the threshold for fiber destruction was not reached.

Reference [84] showed the possibility in principle of the quasi-CW propagation of an OD along a revolver hollow-core optical fiber with a mean velocity of about 1 m s^{-1} over distances of ~ 1 m under the action of pulsed-periodic radiation with a mean power of about 2 W (with a wavelength of 1064 nm). Using nanosecond pulses of a relatively complex shape (each 130-ns pulse was a sequence of individual 100-ps pulses) makes it possible in principle to obtain information on the processes occurring in HCFs during OD propagation from the pattern of its core damages, which is impossible in the case of its complete destruction, as, for example, in [89]. In the experiments [78], the laser radiation intensity on the fiber axis reached 2×10^{12} W cm^{-2} in the maxima of picosecond pulses. However, no optical breakdown was observed in this case, so it was necessary to initialize OD especially to observe the process of optical fiber destruction, as in the majority of such experiments (see, e.g., [83]).

Reference [78] presents the first detailed study of the phenomenon of catastrophic destruction of hollow-core optical fibers exposed to pulsed laser radiation. To construct the physical picture of OD propagation along an HCF, the analysis of fiber damages arising during OD movement was applied, as was earlier done in Ref. [91]. Changing the medium surrounding the silica structure of the revolver optical fiber (ROF) allowed detecting the drastic dependence of the mean OD propagation velocity along the hollow-core optical fiber on the properties of the environment. Note that such a phenomenon has never been detected in OD propagation through conventional all-solid-state fibers (see, e.g., review [79]).

3.2.1 Experimental setup to observe the effect. A schematic diagram of the experiment is presented in Fig. 11a. It is like the one used in Ref. [84]. Through the lens *1*, the laser radiation enters the core of the ROF about 50 cm long or more with the input efficiency of 80%. The experiments were

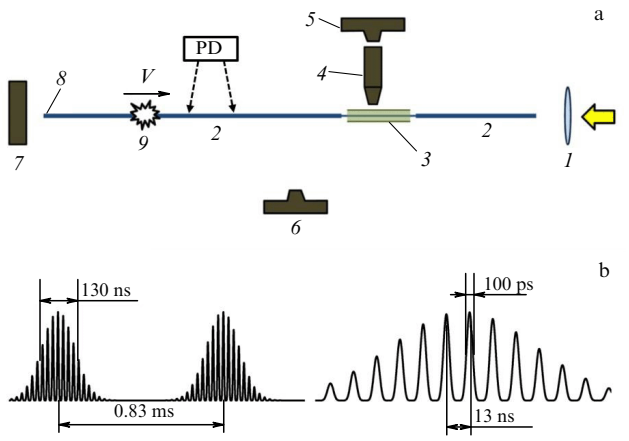

Figure 11. (a) Experiment schematic diagram. (b) Laser radiation parameters. Left — parameters of nanosecond trains of picosecond pulses, right — parameters of picosecond pulses (not to scale).

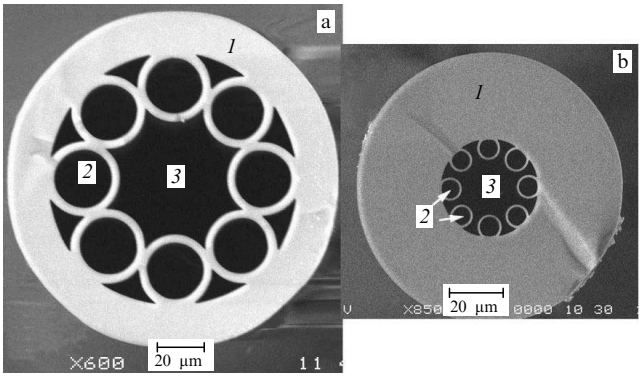

Figure 12. Images of ROF1 (a) and ROF2 (b) cross sections. *1* — support tube; *2* — capillaries of reflective cladding; *3* — hollow core. Basic geometrical dimensions (ROF1/ROF2): support tube outer diameter 125 μm/100 μm, hollow core diameter 42 μm/20 μm, support tube inner diameter 93 μm/36 μm, reflective cladding capillary wall thickness 3.1 μm/0.8 μm, support tube wall thickness 16 μm/32 μm.

carried out with ROFs of two types, ROF1 and ROF2. In both cases, the optical fiber was a fused silica structure with a polymer coating. The cross section of ROF1 and ROF2 silica structures are shown in Fig. 12. In some cases, the polymer coating was removed from segments of the optical fiber. Particularly, in several experiments, in the segment *3* (Fig. 11a), the polymer coating of ROF2 was removed to place this segment in an immersion liquid and to observe the process of OD propagation with microscope *4*. The image was recorded with camera *5*, the shutter of which was open during the whole time the OD moved in the camera field of view. In addition, the process of OD propagation was recorded by TV camera *6* with at a rate of up to 240 frames per second. In the chosen ROF 30-mm-long segment, the OD plasma glow was recorded by a photodiode (PD). After the OD initiation near the output end face of fiber *8* (by contacting the output face with a metal plate), the movement of OD *9* along the air-filled core of the optical fiber began with the average velocity V. The arrow indicates the direction of OD propagation. Note that, without initiating, no OD occurred in our experiments, and the radiation passed through the entire segment of the ROF without visible perturbations.

The Nd:YAG laser served as a source of single-mode radiation. The laser operated in the combined Q-switch and mode-locking regimes and generated nanosecond trains of picosecond pulses (NTPPs) with the parameters indicated in Fig. 11b. Power values of up to 1 MW were reached in the maxima of picosecond pulses (PPs), which allowed observing OD in revolver optical fibers. The average power of laser radiation P_{av} at the ROF output when initiating the OD amounted to about 4 W for ROF1 and 2 W for ROF2. The average power in nanosecond pulses was 16 (8) kW at the output of ROF1 (ROF2) and at the maxima of PPs it reached 2.0 (1.0) MW, which corresponds to a laser radiation intensity at the core axis of the ROF1 (ROF2) fibers of 2.4×10^9 (5.2×10^9) W cm^{-2} averaged over the NTPPs and 3.2×10^{11} (7.0×10^{11}) W cm^{-2} in the PP maximum, respectively.

The wavelength of the Nd:YAG laser was in the transparency regions for both ROF1 and ROF2. Optical losses in the fibers at this wavelength were substantially below 1 dB m^{-1} and, in fact, did not affect the propagation of radiation through the used short segments of the ROF. The OD was initiated in ROFs of both types.

3.2.2 Description of optical discharge propagation. After launching laser radiation into the ROF (4 W into ROF1 and 2 W into ROF2), the OD was initiated and then propagated along the fiber with a velocity of ~ 1 m s^{-1}. The OD was seen as a spot brightly shining in the visible range that moved along the fiber towards the source of laser radiation. Although the laser operated in the pulsed regime and the duration of nanosecond pulses (more precisely, NTPPs) amounted to nearly 10^{-4} of the time separating them, on average the OD moved along the optical fiber with a nearly constant mean velocity (averaged over a few periods between NTPPs). It is interesting that by order of magnitude it turns out to be nearly the same as that of the OD in standard silica fibers with a solid core under the action of CW laser radiation having a similar mean power P_{av} [81]. Figure 13 presents a photograph of an OD propagating along ROF1 with an exposure of (1/120) s. The motion of the OD along the ROF1 is directly represented in the video record made with camera *6* with a deceleration of about 10 times [92].

The results of OD propagation through the optical fibers ROF1 and ROF2 were substantially different. **In the case of ROF1**, after OD passage, the silica fiber structure was fully destroyed, and its fragments were kept together only by the polymer coating. This led to a change in the equilibrium conditions of the ROF1 fiber, which during the experiment was fixed in the hanged state (see Fig. 13). Therefore, in the

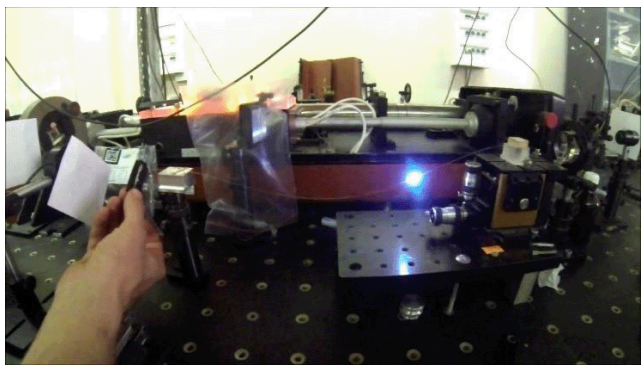

Figure 13. Photograph of OD propagating along ROF1 shot by camera *6* (Fig. 11a) with an exposure of (1/120) s. Point of laser radiation input into ROF1 is on the right, point of OD initiation is on the left.

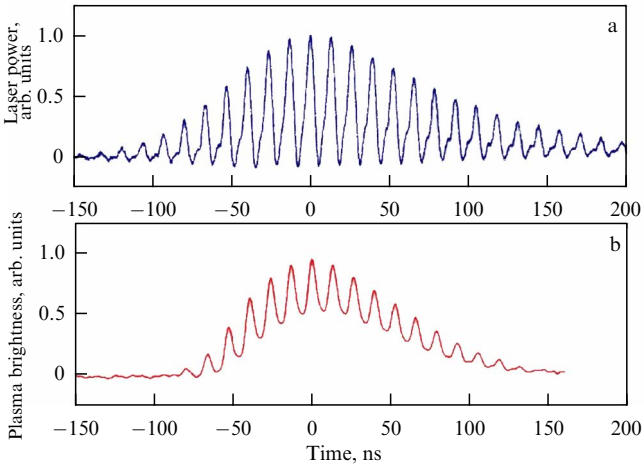

Figure 14. (a) Oscillogram of NTPP radiation from a Nd:YAG laser. The NTPP consists of 100-picosecond pulses, repeating with a period of 13 ns. Real duration of a PP is not seen in the oscillogram because of the limited frequency band of the recording circuit. (b) Oscillogram of OD plasma glow in ROF2 under exposure to NTPP laser radiation.

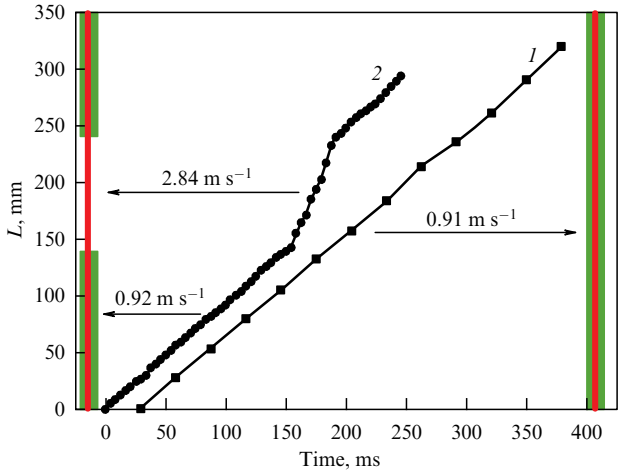

Figure 15. Time dependence of path length L passed by the OD along the core of ROF2 fully coated with polymer (*1*) and partially cleaned of polymer (*2*). On the right and on the left, ROFs are shown partially and fully coated with polymer, respectively. Measured mean velocities of OD propagation on various segments of the fibers are indicated.

process of OD propagation, mechanical vibrations of the ROF1 fiber were excited (which can be considered a manifestation of a certain 'optomechanical effect'; see [92]). Note that, in the process of optical discharge propagation in the CW regime along hard-core silica fibers with the same mean velocity, no movements of the whole fiber (and its vibrations) are observed, in full agreement with the laws of mechanics (a video of a discharge traveling along a communication fiber in the CW regime can be seen, e.g., in Ref. [93]). If during the propagation along ROF1 the OD appeared in the segment with a preliminarily stripped polymer coating, the optical fiber was destroyed, and the OD propagation stopped (which is confirmed by the ROF1 fiber breakage in the end of the video record [92]). Apparently, when the silica structure of ROF1 is broken, the pressure of heated air in the fiber core falls, increasing the laser radiation absorption length in the hollow core of the ROF1 and disturbing the gas motion in the core, which ultimately leads to a violation of the OD initiation process by the next NTPP and, therefore, stops the OD. It should be noted that this phenomenon can be used to protect communication lines based on hollow-core optical fibers. For this purpose, it is sufficient to provide in the line a segment of optical fiber with a sufficiently thin support tube, cleaned of polymer. Then, the OD that has arisen for some reason will stop on arrival at this segment, thus protecting the rest of the fiber system from damage.

In the case of ROF2 with the wall of the carrying tube twice as thick (see Fig. 12), the fiber after the OD passage preserves visible integrity. Saving the main elements of the ROF2 structure after the passage of OD allowed studying the damage to the fiber structure caused by the OD and extracting information about the processes that take place during OD propagation from the form of damage produced.

A comparison of oscillograms of the laser radiation and the OD plasma glow in the visible spectral range shows that in most cases the OD plasma glow correlates with the laser radiation. Typical oscillograms are presented in Fig. 14. The comparison of oscillograms in Figs 14a and 14b shows that during the pause between PPs the OD plasma does not fade and the number of laser PPs supporting the propagation of OD is substantially less than the whole number of pulses in the NTPP. The OD is maintained only by PPs with a high enough amplitude. PPs manifest themselves as peaks of the OD plasma flow, but the oscillogram of the OD glow (b) also has a 'constant' (on the nanosecond time scale) component. Therefore, the time constant of OD plasma relaxation exceeds 13 ns, the interval between the adjacent picosecond pulses. But between NTPPs the plasma glow is absent. Every new train of picosecond pulses initiates the formation of plasma in the fiber core. From a comparison of Figs 14a and 14b, an estimate follows that the OD arises at a laser radiation intensity equal to $\approx 20\%$ of the maximum intensity in picosecond pulses.

However, in some cases, the number of maxima of the OD glow during one NTPP reduces to a few units (the number of corresponding maxima in Fig. 14b is 17). And in a few cases, the glow of the OD plasma is not observed at all: some kind of NTPP 'skips' appear in the oscillograms of the OD glow. At present, such variations in the OD plasma behavior seem random, with the frequency of occurrence of $\sim 10\%$. Their origin requires additional investigation.

It was found that, at $P_{av} \leqslant 1.0$ W, no OD initiation or propagation along the ROF2 was observed in any cases. But at $P_{av} \geqslant 1.5$ W, OD propagation was observed in all experiments. The corresponding intensity values in the maxima of PPs on the ROF2 axis amount to 3.5×10^{11} W cm$^{-2} \leqslant I_{th} \leqslant 4.7 \times 10^{11}$ W cm^{-2}.

The velocity of OD propagation along the fiber was determined from the data of video recording with camera *6* (Fig. 11a). It turned out that the average velocity of the OD motion V_{av} substantially depends on whether the ROF is coated with a polymer or not. In the case of ROF2 fully polymer coated, the time dependence of the path length traveled by the OD corresponded to motion with an approximately constant average velocity (Fig. 15, line *1*), in this case $V_{av} = 0.91$ m s^{-1}. However, if the polymer coating was removed from a part of ROF2 and the silica structure of the fiber was in direct contact with air, then, unlike in ROF1 with a less strong silica cladding, OD also propagated over this section of ROF2 without destroying it, but with

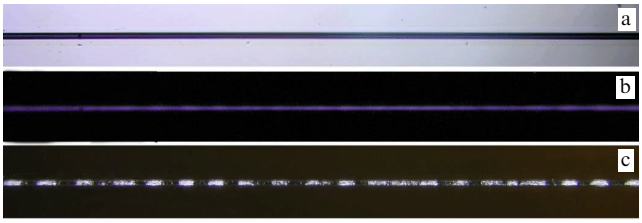

Figure 16. Photograph of the same ROF2 segment before (a), during (b), and after (c) the passage of an OD through it. In all three cases, the fiber without a polymer coating was in an immersion liquid. (a) Illumination from below; (b) intrinsic OD glow; (c) side illumination; total width of each frame is 3.5 mm.

significantly higher values of V_{av}. The time dependence of the path length traveled by the OD $L(t)$ in this case had the form of a polygonal line (Fig. 15, line *2*), different segments of which corresponded to motion with a velocity of $V_{av} = 0.92$ m s^{-1} (on the segment with the polymer coating) and $V_{av} = 2.84$ m s^{-1} (on the segment without coating), i.e., ≈ 3 times faster. This result has been multiply reproduced in experiments. Its possible explanation, associated with the difference in the coefficient of shock waves reflection from the silica–air and silica–polymer interfaces, is presented in Ref. [78].

Figure 16 presents photographs of one and the same segment of the ROF2 fiber before, during, and after the OD passage shot with camera *5* (see Fig. 11). Before the OD passage, the fiber is uniform in length (Fig. 16a). The time–integrated photograph of OD plasma glow (Fig. 16b) (the shutter of the camera was open the entire time the OD was in the field of view of the camera) testifies that the OD on the presented segment propagated continuously through the hollow core of ROF2. In the photograph shot after the OD passage (Fig. 16c), the destruction of the reflective ROF2 cladding is fixed, which has a structure close to periodic with a period of about $\Delta = 180$ μm. Within each period (where the periodicity holds), the segments with significant damage of the reflective cladding capillaries (light in Fig. 16c) alternate with less damaged segments, where the capillaries have been saved with practically no defects (dark in Fig. 16c).

3.2.3 Physical processes responsible for optical discharge propagation along a hollow-core fiber. The above experimental results can be explained as follows (Fig. 17). Immediately after the initiation (plasma formation in the hollow core of the fiber using a metallic target), under the action of a laser picosecond pulse (PP), a light-supported detonation wave (LSDW) propagates with velocity [94]

$$V_{LSDW} = \left[2(\gamma^2 - 1)\,\frac{I_p}{\rho_0}\right]^{1/3} \qquad (4)$$

and passes the distance $S_{LSDW} = V_{LSDW}\,t$. Here, ρ_0 is the air density in the core of the ROF, I_p is the radiation intensity in a picosecond pulse, γ is the adiabatic exponent, and t is the time. Under the conditions of the experiments considered, $V_{LSDW} \sim 300$ km s^{-1} and $S_{LSDW}(\tau_p) = 30$ μm.

After the PP end, the light-detonation wave is no longer supported by the laser radiation and now continues its movement as a damped shock wave (SW). Its path length in Fig. 17 is denoted by S_{SW}. The traversed path length is in best correspondence with the path length passed by a spherical shock wave from a point explosion with energy E equal to the

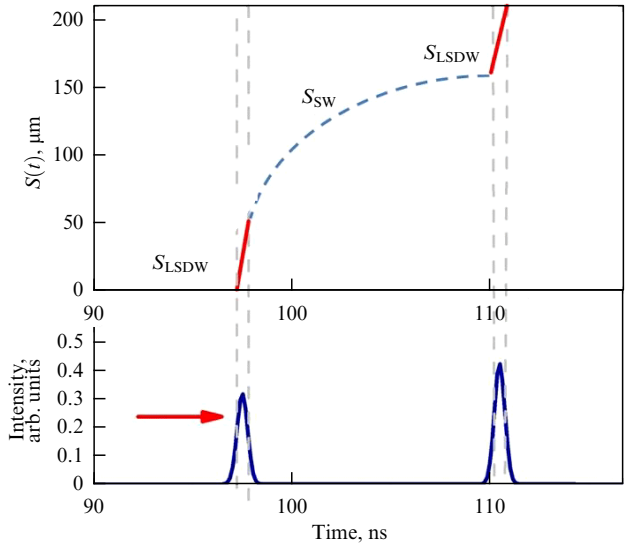

Figure 17. Schematic of OD propagation along an HCF. Bottom — picosecond pulses of laser radiation (depending on time), top — path length passed by the OD depending on time.

energy of the picosecond laser pulse [95]

$$S_{SW} = \left(\frac{E}{\rho_0}\right)^{1/5} t^{2/5}. \qquad (5)$$

This yields the path length passed by the OD during the period between two picosecond pulses $\Delta = S_{LSDW} + S_{SW} = 130$ μm, which, bearing in mind the approximate character of numerical estimates performed, is close enough to the value of $\Delta = 180$ μm observed experimentally.

The next PP, which comes in 13 ns, comes to be absorbed at the leading edge of the SW with the power still high, as a result of which the process of LSDW formation and relaxation repeats. In the HCF segments where the pressure step in the LSDW and SW is high enough, the destruction of capillaries forming the reflective cladding of the HCF occurs. In the regions between them, no destruction of capillaries is observed. After the end of the HTPP, the OD plasma in the core completely relaxes and the OD plasma propagation under the action of the next NTPP begins from the very initiation. In this case, the OD can be initiated in a region containing fragments of destructed capillaries at the expense of increasing the electric field strength in sharp pieces of fused silica.

The experimental data obtained show that, to support the OD propagation regime along a hollow-core optical fiber, much higher threshold values of the laser radiation intensity are required: more than 10^{11} W cm^{-2} (recall, for comparison, that, for the OD propagation along a solid-core fused silica fiber, an intensity substantially lower than $\sim 10^6$ W cm^{-2} is required).

4. Nonlinear optics in gas-filled hollow-core optical fibers

4.1 Nonlinear compression and generation of ultrashort laser pulses in hollow-core optical fibers

The generation of ultrashort pulses (USPs) in hollow-core optical fibers has been a dynamically developing problem for

a few ten years already [96, 97]. The spectral broadening of pulses necessary to reduce the pulse duration in an HCF is reached due to a nonlinear interaction between laser pulses of high intensity and the gas medium filling the core of the HCF. The main nonlinear effect responsible for the spectral broadening is self-phase modulation (SPM). It is known that nonlinear changing the wave phase in time leads to a change in its frequency; therefore, when a pulse propagates through a Kerr-nonlinear medium, its spectrum is broadened, which is accompanied by the inducing of a linear chirp (carrier frequency modulation) [98]. The first HCFs that were used to compress laser pulses were hollow-core fibers of fused silica with a small length (60–70 cm) and large hollow core radius (140–160 μm) [96, 99]. Using systems based on such HCFs, few-cycle laser pulses exceeding in energy the pulses obtained earlier by more than three orders of magnitude were obtained. The generation of femtosecond pulses of such duration and with such values of energy compared to the generation in optical fibers with a solid-state core of fused silica has been achieved due to two main factors. First, the nonlinear coefficient n_2 in noble gases filling the core of HCFs was nearly three orders of magnitude less than that in fused silica. Second, the size of the fiber core was significantly increased in correspondence with the scaling law for peak powers of the launched laser pulse [97]. Ref. [99] proposed a scheme for pulse compression based on the SPM effect in HCFs of fused silica with the core filled with krypton and argon. The gases were at a pressure of the order of 2 atm. Pulses from a titan–sapphire laser at a wavelength of 780 nm with a duration of 20 fs were used. The pulse energy was of the order of 40 μJ. As a result of interacting with the gaseous medium, spectrally broadened pulses were obtained at the output of the hollow-core fiber, which were directed to a system of two prisms of fused silica and compressed to 4.5 fs, the pulse energy being 15 μJ. In addition, the system used a chirped mirror to compensate for phase distortion during pulse propagation through the hollow core and a sequence of compressor prisms. Despite the energy loss, the peak power in the pulse increased. In this case, a problem arose related to the multimode property of such a hollow-core waveguide, which was solved by choosing the regime of input laser beam focusing. Thus, an HCF-based compressor together with a chirped mirror to compensate for dispersion became one of the key technologies for generating high-intensity laser pulses with a few oscillations of the electromagnetic field [100]. Based on a similar scheme and an HCF with the core surface coated with layers of silver and polymer, the authors of Ref. [101] managed to compress input pulses with a duration of 100 fs and energy of 1–2 mJ at a wavelength of 785 nm to a duration of $\sim$ 20 fs with energies up to 300 μJ. The HCF core was filled with air at atmospheric pressure, and the main problem due to this fact was a strong shift of the pulse spectrum towards the long-wavelength region due to intrapulse Raman scattering. This is exactly why silver and polymer coatings made a necessary contribution to the dispersion properties of the HCF core mode, ensuring successful pulse compression.

Among the latest achievements in using fused silica HCFs with thick walls and large hollow core diameters, it is worth mentioning the generation of pulses with several oscillation periods in the mid-IR spectrum range [102]. For this purpose, a straight HCF filled with krypton with a hollow core diameter of 1 mm and length of 2.8 m was chosen, outside which an external grating-pair compressor was placed. Two pulses with an energy of 2.8 mJ and duration of 160 fs at a wavelength of 4 μm were launched into the HCF from a parametric amplifier. As a result of spectrum broadening by approximately an octave due to SPM and further compression, pulses with a duration of 22.9 fs and an energy of 2.7 mJ were obtained at the output.

The above compressors of laser pulses allowed reaching the maximum energies in the compressed pulses at a level of a few mJ, but their duration could not be less than a few ten femtoseconds [103]. This is because the geometric parameters of the HCFs used, i.e., an outer diameter of 1–2 mm and core diameter of the order of a few hundred micrometers, allowed using them in the straight shape only. In addition, they had to be situated in special metallic V-grooves, the length of which commonly did not exceed 1 m. Naturally, this reduces the possibility of SPM spectrum broadening. To extend the capabilities of transmitting short femtosecond pulses with high energy, the authors of Ref. [104] proposed using HCFs in the form of capillaries, but with a much thinner wall. They were called stretched flexible hollow-core fibers. In experiment [104], they used fused silica capillaries two meters long with a hollow core diameter of 320 μm. It was demonstrated that, when feeding this HCF with femtosecond laser pulses of a Gaussian shape with a duration of 120 fs and energy of 120 μJ, due to the SPM effect, it is possible to obtain output pulse compression to 10 fs. Note also Ref. [105], in which in a similar two-meter HCF in the form of a silica glass capillary with a helium-filled hollow core diameter of 450 μm and pulses with a duration of 4 fs with 3 μJ of energy were obtained. Circularly polarized radiation in the form of pulses with a duration of 23 fs and energy of 8 μJ were delivered to the HCF input. For a more efficient compression process in the HCF hollow core, a pressure gradient in the helium was created. In the presence of a pressure gradient in the gas filling the core of the fiber, the nonlinear interactions in the gas increase gradually, thus reducing the probability of self-focusing and gas ionization.

The approach to compressing laser pulses in HCFs with external compressors in the form of gratings and chirped mirrors has also been extended to microstructured HCFs. The first microstructured HFCs used to compress laser pulses were those with Kagomé cladding and negative curvature of the core–cladding interface [106]. The HCF was filled with xenon at a pressure of 8 atm. In this paper, the authors spectrally broadened picosecond pulses from a disk mode-locked laser at a wavelength of 1.03 μm and compressed them to durations of less than 250 fs and energies of the order of 1 μJ (Fig. 18). In another paper [107], using an HCF with negative curvature of the core–cladding interface and photonic-crystal Kagomé cladding, pulses with a duration of 330 fs and energy of 70 μJ from a Yb laser were compressed.

The pulses were compressed to durations of 34 fs and an energy of 50 μJ in an HCF with the core diameter of 40 μm filled with air at atmospheric pressure. The HCFs made of fused silica with negative curvature of the core–cladding interface and with cladding consisting of capillaries are also widely used to compress laser pulses. In Ref. [108], the compression of femtosecond laser pulses occurred in two stages and was used to generate ultrashort pulses in the deep ultraviolet with an energy of the order of 1 μJ. Such pulses were generated due to the appearance of dispersive waves in the propagation of solitons, arising due to self-compression in HCFs filled with a mixture of neon and helium. In this case, the solitons themselves were generated via the pumping of the

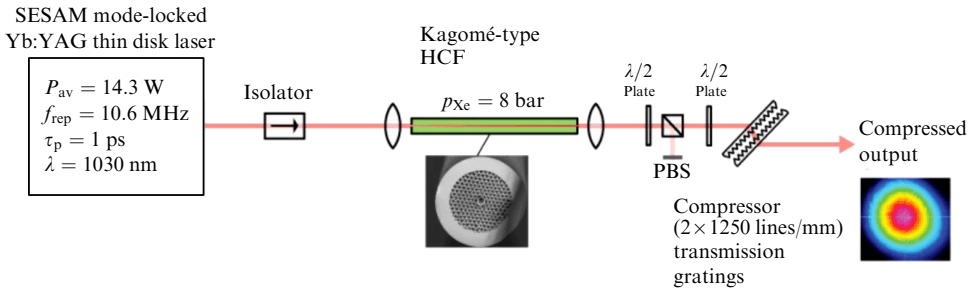

Figure 18. Compression of picosecond laser pulses in an HCF with Kagomé cladding. (Adopted from Ref. [106].)

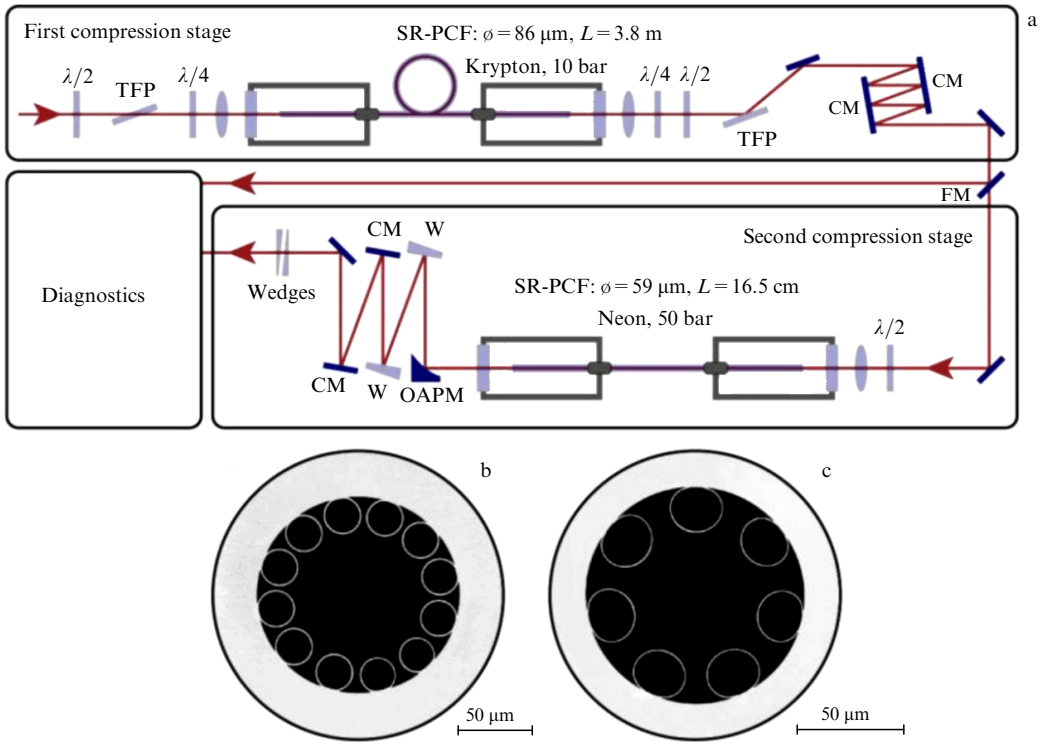

Figure 19. Schematic of two-stage compression of femtosecond laser pulses in an HCF with cladding consisting of capillaries. An HCF with nine capillaries was used in the first stage and an HCF with seven capillaries in the cladding was used in the second stage of the setup. (Adopted from Ref. [109].)

HCF with ultrashort laser pulses < 25 fs, created by compressing 300-fs pulses from an ytterbium fiber laser, launched into another HCF filled with argon. The pressure of gases in both HCFs was regulated to achieve an optimal regime for the generation of ultrashort pulses. At the output of the first HCF, a system of chirped mirrors was used to compensate for the dispersion and the positive chirp occurring in the first HCF in the process of SPM. A similar two-stage pulse compression scheme was used in Ref. [109]. In different stages, HCFs with different hollow core diameters and different numbers of capillaries in the cladding were used (Fig. 19). In the present case, in the first stage, comprising an HCF and chirped mirrors, a compression of the laser pulse from an ytterbium laser with a duration of 340 fs to 25 fs occurred. The first HCF was filled with krypton, and the diameter of its core was 86 μm. At the output of the second HCF with the core diameter of 59 μm, filled with neon, a pulse with the duration of 3.8 fs, which amounted to 1.25 of the optical oscillation period, was obtained. The pulse energy was 5 μJ.

Worth noting is also recent paper [110], in which the authors compressed a 250-fs pulse at a wavelength of 1.03 μm to 13.3 fs in an HCF filled with xenon. The energy of the input pulse was 3.8 μJ, and the energy of the output pulse was 2.7 μJ. The setup comprised external chirped mirrors, as in the above examples.

In Ref. [111], picosecond pulses from a holmium laser (Ho:YLF) with a power of a few mJ were compressed to pulses with a duration of the order of 300 fs at a wavelength of 2050 nm in an HCF with negative curvature of the core–cladding interface and Kagomé cladding. The HCF core was filled with argon. SPM was the main nonlinear process that led to pulse broadening. At the HCF output, there was an outer compressor consisting of two prisms, which allowed pulse compression to 285 fs with the energy being 125 μJ. Two-stage systems for laser pulse compression were successfully applied in the mid-IR spectral range. The authors of Ref. [112] used the same approach as in Ref. [111] to compress picosecond pulses from an Ho:YLF laser at a wavelength of 2050 nm. In this case, they used the second HCF in the system for the self-compression of the laser pulse. As a result of passing 3.3-ps pulses with an energy of 140 μJ through the first HCF with Kagomé cladding and negative curvature of the core–

cladding interface, followed by an additional compression system of prisms, a pulse with a duration of 285 fs and an energy of 90 μJ was obtained. As a result of self-compression when passing through the second HCF with an air-filled core, the pulse duration became 48 fs.

In addition to the approach described above, an approach to laser pulse compression in HCFs due to the presence of anomalous dispersion in them in the necessary spectral range has found application. In this case, the self-compression of laser pulses occurs in the soliton regime. This issue was partially discussed above for two-stage schemes of generating ultrashort laser pulses. It is exactly this technique which is believed to allow obtaining the shortest pulses with durations of less than a period of optical oscillation and a multioctave spectral width [97]. On the other hand, it has been pointed out that in this case complex nonlinear processes occur, which are very sensitive to the parameters of the laser pulse entering the system. The main difficulty is to choose necessary values of energy of the pulse input in the system and the corresponding peak powers. The mechanisms of self-compression of laser pulses in an HCF without external dispersion-compensating elements in the experimental setup was demonstrated for the first time in Ref. [113]. In this case, a 30-fs pulse with an energy of 2.2 μJ was focused on an HCF only 2.5 cm long and with the hollow core diameter of 150 μm. The HCF was filled with argon at a low pressure. The calculation showed that the radiation intensity in the HCF was at a level of 10^{15} W cm^{-2}, quite enough to ionize the gas at the leading edge of the pulse. At this level of radiation intensity, the fast ionization of the gas at the leading edge of the pulse leads to a fast decrease in the plasma refractive index, which, in turn, leads to a strong shift of the pulse spectrum towards the shortwave region accompanied by the appropriate spectrum broadening. An important role in pulse propagation is also played by the self-steepening effect. Thus, the pulse duration at the HCF output could be reduced to 13 fs without using any external dispersion compensators.

As mentioned above, the main mechanism of self-compression of laser pulses with energies of the order of a few μJ is based on forming high-order solitons in an HCF with anomalous dispersion. Reference [114] theoretically predicted the possibility of supporting the soliton mode of pulse propagation in microstructured HCFs with Kagomé cladding. The theoretical calculations were experimentally confirmed in Ref. [115], where the authors demonstrated the spectral broadening of a 30-fs pulse with an energy of 1 μJ, introduced in an HCF with Kagomé cladding. In this case, the excitation of dispersive waves was also observed, which gave rise of spectrum broadening in the HCF up to wavelengths lying in the deep ultraviolet. Further work in this area has led to obtaining pulses with a duration of 1.7 of the optical cycles at a wavelength of 800 nm [116]. In the experiment, a 10-cm-long HCF with Kagomé cladding was also used. The core of the HCF 30 μm in diameter was filled with argon or krypton. As a result of soliton self-compression in the HCF, pulses with a duration of less than two periods of optical wave oscillations and an energy of 1 μJ per pulse were obtained. The process of soliton formation was accompanied by the emission of dispersive waves. An efficient system of soliton self-compression of pulses was also obtained in an HCF with Kagomé cladding and negative curvature of the core–cladding interface. The HCF length was 20 cm and the diameter of the fundamental mode was ~ 64 μm [117]. Here, a very simple scheme was used, shown in Fig. 20.

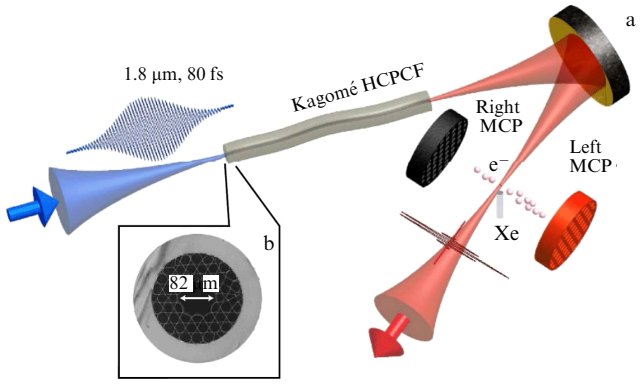

Figure 20. Schematic of a setup for soliton self-compression of laser pulses in an HCF with Kagomé cladding and negative curvature of the core–cladding boundary. An electron spectrometer with two detectors is shown at the beam output. (Adopted from Ref. [117].)

The pump was implemented using a parametric amplifier with a tunable wavelength of 1.4–1.9 μm, which produced 80-fs pulses with energies of up to 120 μJ. The HCF core was filled with xenon at a pressure of 4 atm. As a result of compression, pulses as long as one period of the optical wave with energies of up to 100 μJ were obtained. It is worth noting that the effective soliton self-compression of laser pulses is also possible in the short-wave spectral region. In Ref. [118], pump pulses with an energy of 2.6 μJ and duration of 54 fs at a wavelength of 400 nm were compressed to a duration of 11 fs. In this case, the core of the HCF with Kagomé cladding was filled with the surrounding air and had dimensions that allowed reaching a sufficient level of anomalous dispersion.

To finalize this review of the generation of ultrashort laser pulses, it is worth mentioning Ref. [119], where the role of an HCF was played by conventional glass capillaries. The authors of Ref. [119] experimentally demonstrated that, when 10-fs pulses with an energy of 337 μJ from a titanium–sapphire laser are launched into a capillary filled with helium at a pressure of 0.4 atm, soliton self-compression makes it possible to obtain pulses with a duration of 1.2 fs with a possibility of proceeding to the attosecond region of pulse durations. The capillary of fused silica was 3 m long with a core diameter of 250 μm.

The supercontinuum generation in HCFs of various types could be a logical continuation of describing various modes of generating ultrashort laser pulses in such HCFs. First of all, we would like to mention studies where the supercontinuum generation was accompanied by the emission of dispersive waves, which, in turn, gave rise to the generation of pulses in the deep ultraviolet region. In Ref. [120], the authors obtained supercontinuum generation from the deep ultraviolet to near-infrared in the wavelength range from 113 to 1000 nm. An HCF with a Kagomé cladding having a core diameter of about 30 μm was filled with helium or neon. The pumping was implemented with 35-fs pulses at a wavelength of 800 nm from a titanium–sapphire amplifier. The energy of the input pulses varied from hundreds of nanojoules to tens of microjoules. The pressure in the HCF core could vary up to 30 atm. It was found that there are several basic mechanisms leading to the generation of high-frequency components in the pump pulse at the wavelength of 800 nm. In the experiment considered, it was possible to reveal two of them:

the appearance of coherent radiation in the form of dispersive waves in the visible spectral range and up to the deep ultraviolet (180–550 nm), as well as a frequency shift in the generated soliton to the short-wave side, arising due to photoionization in the gas. It is known that the generation of dispersive waves at high frequencies from a compression soliton arising from a pump pulse can be interpreted as a cascade four-wave mixing process. Ignoring dispersion terms higher than those of the third order, we can express the dispersive wave frequency as

$$\omega_{\mathrm{dw}} = \omega_{\mathrm{sol}} + \frac{3|\beta_2|}{\beta_3}\,, \tag{6}$$

where ω_{sol} is the soliton central frequency, β_2 is the group velocity dispersion, and β_3 is the third-order dispersion, both of the last two terms taken at the pump frequency. As the frequencies approach those of electronic transitions in the gas, it becomes necessary to add higher-order dispersion terms to Eqn (6), which changes the phase matching conditions. To generate dispersive waves at a wavelength of < 200 nm when pumping at a wavelength of 800 nm, it is necessary to have a wavelength of zero dispersion at wavelengths of < 400 nm. In experiments, this was reached by means of changing the gas pressure in the HCF core, choosing the optimal value of the core diameter. Thus, in addition to the generation of a supercontinuum in a wide range of the spectrum, ultrashort dispersive waves in the HCF with a Kagomé cladding and a hollow core filled with helium and neon were obtained. Emission of dispersive waves was observed in the range from 120 to 200 nm in pulses with an energy of about 50 nJ, with an efficiency of about 1%.

In Ref. [121], the authors complicated the structure of the fused silica Kagomé cladding by introducing additional thickenings of bridges near the boundary of the hollow core. This allowed obtaining supplementary peculiarities of the HCF waveguide dispersion, since the bridges provided new resonances in the HCF transmission spectrum, in addition to the proper resonances determined by the wall thickness of the Kagomé cladding. As a consequence, they managed to find four zero-dispersion wavelengths in the desired spectral intervals and to control the supercontinuum spectral characteristics. An HCF with a core diameter of 50 μm was filled with krypton at a pressure of 6 atm. The supercontinuum was excited by 80-fs pulses at a wavelength of 800 nm and had a width from 200 nm to 1700 nm.

Besides the HCFs with Kagomé cladding, HCFs of fused silica with the cladding consisting of capillaries were also used to generate a supercontinuum. The authors of Ref. [122] observed supercontinuum generation simultaneously in several transmission bands of an HCF with a cladding consisting of eight capillaries. The hollow core diameter was equal to 61.5 μm, the core was filled with air at atmospheric pressure, and 205-fs pulses with an energy of 110 μJ at a wavelength of 1028 nm were introduced in it. As a result, the generation of a supercontinuum was observed in 11 transmission bands of the HCF, and its spectral width was from 415 to 1593 nm. It was theoretically predicted that its width can be extended to 4200 nm. An interesting result on supercontinuum generation in several HCF transmission bands [123] was obtained using a fused silica fiber consisting of seven capillaries and having a hollow core diameter of 44 μm. The core of this HCF was filled with argon with a pressure of up to 30 atm. Pumping pulses with a duration of 100 fs and energy of 8 μJ were introduced in the center of the most longwave transmission band with the wavelength of 2460 nm. As a result, the spectral width of the supercontinuum was from 200 nm to 4000 nm with the output energy at a level of 8 μJ. As was described above, these were the processes of efficient self-compression of solitons due to nonlinear soliton–plasma interactions and the corresponding generation of dispersive waves in the ultraviolet spectral region that could lead to such a supercontinuum spectral width.

Finally, we should mention Ref. [124], in which a supercontinuum from 400 nm to 1200 nm was obtained in a fused silica HCF with a hollow core diameter of 26 μm and six capillaries in the cladding. The core was filled with nitrogen at a pressure of 40 atm, and the HCF length was 10 m. A laser at a wavelength of 532 nm with a pulse duration of 20 ps served as a pump source. An additional continuum was observed in the spectral range from 250 nm to 360 nm. In this case, the supercontinuum was due to the excitation of a broad Raman frequency comb corresponding to the vibrational transitions in nitrogen molecules. This process was supplemented with a strong contribution from the Kerr nonlinearity of the medium.

4.2 Gas fiber lasers and mid-infrared range development

The invention of hollow-core optical fibers opened the way to developing a new type of laser — the gas fiber laser (GFL) Using the gas filling the fiber hollow core, such radiation sources can combine the advantages of fiber lasers (compactness, low lasing threshold, single-mode radiation) and gas lasers (high output power, narrow lasing line).

During the last ~ 10 years, the most intense development was of GFLs lasing in the mid-IR range at wavelengths above 2 μm, which is due to a combination of several factors. First, the mid-IR range is of great interest for practical applications, because it covers the absorption lines of many chemical compounds. Second, the current state of hollow-core fiber technology already allows fabricating fibers with fairly low optical losses in the spectral range of 2–5 μm. In this case, it is important that the microstructured HCF cladding fabrication is based on the well-developed fused silica technology. And third, gas mixtures as active media for GFLs offer a wide choice of laser transitions in the mid-IR range.

The pumping of gas active media can, in principle, be implemented in various ways, including pumping with optical (laser) radiation, gas discharge, or chemical reactions. However, almost all GFLs implemented practically use optical pumping, which is considered in more detail in Section 4.2.1. The first gas discharge GFL in the world was demonstrated only in 2023 as a result of collaborative work of two laboratories of the Prokhorov General Physics Institute, namely, the Laboratory of Hollow-Core Optical Fibers and the Laboratory of Gas Discharge Lasers. Gas discharge GFLs are considered in more detail in Sections 4.3. and 4.4.

4.2.1 Gas fiber lasers with optical pumping. The most widespread approach in the design of gas fiber lasers with optical pumping is the use of the single-pass cavity-free configuration (Fig. 21). A solid-state fiber laser can serve as a pump source, which makes it possible to implement an all-fiber GFL design by splicing the fiber output of the pumping laser to the input face of the hollow-core fiber. Nevertheless, in most cases, the pumping laser radiation is introduced into the hollow-core fiber by means of bulk optical elements, which allows

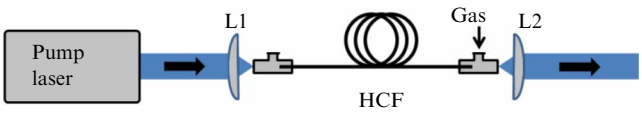

Figure 21. Single-pass cavity-free scheme commonly used to design gas fiber lasers with an optical pump. L1 and L2 are lenses for the radiation input/output from the hollow core of a fiber filled with active gas.

investigating the potential capabilities of GFL, despite the technological problems with splicing hollow-core fibers not having been fully solved yet. The HCF ends are hermetically fixed in miniature gas-filled cuvettes, which have windows for the radiation input/output and allow pumping various gases, which serve as an active laser medium, into the hollow core. In this case, the hollow-core fiber ensures a small diameter of the mode field ($\sim 20-70$ μm) and a large length ($\sim 1-30$ m) of interaction of radiation with the active medium, which allows reaching an optical gain sufficient to excite laser oscillation from quantum noise during a single pass of radiation along the fiber.

Raman gas fiber lasers. Stimulated Raman scattering (SRS) of light in molecular gases filling the hollow core of a fiber is one more method of generating laser radiation, especially in the mid-IR range. SRS not only extends the range of lasing wavelengths available for gas fiber lasers but also simplifies the requirements concerning pump sources, since it is no longer necessary to exactly fit the pumping radiation to fixed narrow absorption lines of the active gas. In fact, well-known near-IR range lasers can be used to pump Raman GFLs, in which the pump photons lose a part of their energy to excite molecular vibrations and the rest of the energy is radiated in the form of a Stokes wave shifted to the longer-wave spectral region. Thanks to large Stokes shifts when using the vibrations of the lightest molecular gases ($\Omega_R = 4155$, 2987, and 2917 cm^{-1} for H_2, D_2, and CH_4, respectively), Raman GFLs offer an opportunity to obtain mid-IR range radiation through a very few Raman cascades. Moreover, the SRS on rotational transitions of molecular gases provides an additional degree of freedom to enrich the output spectrum of Raman GFLs.

The first Raman laser on a photon crystal hollow-core fiber filled with hydrogen was reported in 2002 [125]. In this work, conversion of green radiation (532 nm) into red (683 nm) was implemented via a Raman vibrational transition in the hydrogen molecule, which provide a large Stokes shift (4155 cm^{-1}). However, interest in GFLs soon moved to the near and mid-infrared range, since the SRS in light gases allowed significant spectral shift to the red side, and the hollow-core fibers possess sufficiently low losses in these ranges and allowed operating with high power laser radiation pulses. It should also be noted that the possibility of controlling the HCF transmission spectrum allows controlling the SRS process in molecular gases, e.g., selecting the SRS on rotational transitions of the hydrogen molecule and suppressing the Raman conversion on vibrational transitions that usually develops first. This approach was demonstrated in Ref. [126], where the spectral positioning of high-loss resonant spectral band of the HCF was used to suppress the SRS on a vibrational transition in hydrogen pumped at a wavelength of 1.064 μm with the Stokes component of the SRS on a rotational transition at a wavelength of 1.135 μm.

The first Raman GFL generating in the mid-IR range was demonstrated in 2017 [127, 128]. A revolver hollow-core fiber 11 m long with the core filled with an H_2/D_2 gas mixture at a total pressure of 30 bar was used as an active medium. The pump source was an erbium fiber laser at a wavelength of 1.56 μm, generating pulses with a duration of 3.4 ns, repetition rate of 25 kHz, and average power of 2.4 W. The SRS of pumping radiation on the vibration of D_2 molecules allowed lasing at a wavelength of 2.9 μm in a single pass through the active medium. The quantum efficiency of the Raman GFL amounted to $\sim 10\%$. In addition, the Stokes wave ($\lambda = 2.9$ μm) had enough intensity to serve as a pump for the SRS on rotational transitions of the D_2 and H_2 molecules. As a result, in the output spectrum of the Raman GFL, lasing lines at wavelengths of 3.3 and 3.5 μm were observed.

Further extension of the lasing wavelength of Raman GFLs into the mid-IR range became possible thanks to a reduction in the optical losses in a revolver optical fiber to a value of the order of 1 dB m^{-1} at a wavelength of 4.4 μm. Using this optical fiber filled with pure hydrogen at a pressure of 30 atm, the authors of Ref. [129] demonstrated the first gas fiber laser, implementing a $1.56 \rightarrow 4.4$-μm single-cascade Raman conversion (Fig. 22a).

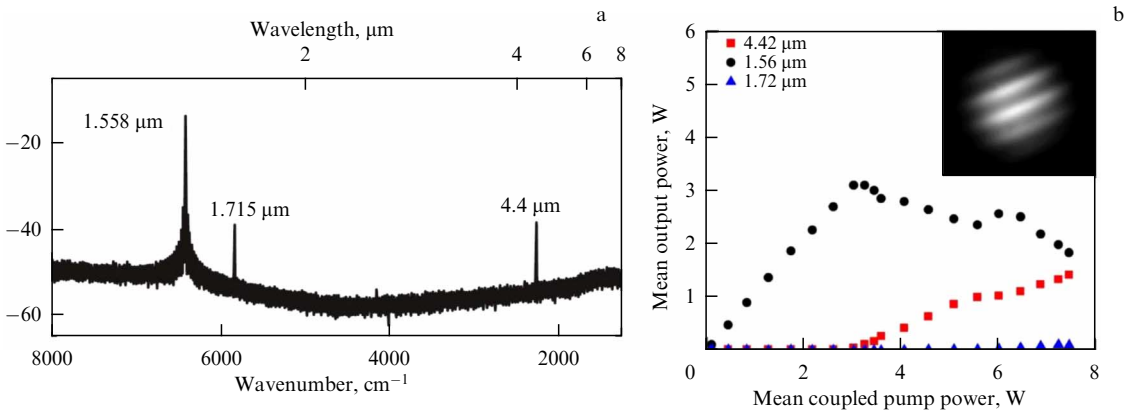

Figure 22. (a) Spectrum of output radiation from a Raman GFL implementing a single-cascade conversion of $1.56 \rightarrow 4.4$ μm [129]. (b) Mean power of various spectral components at the output of the Raman GFL, depending on the introduced pump power. Inset shows transverse distribution of output radiation intensity at a wavelength of 4.42 μm, corresponding to the fundamental mode of the hollow-core fiber [131]. Intensity modulation is caused by interference at the input window of the recording camera.

The quantum efficiency of a Raman GFL lasing at a wavelength of 4.4 μm in the first reports amounted to ~ 15% [129]. In subsequent papers by the same authors, the characteristics of the erbium pump source, the hollow-core fiber length, and the pressure of the active gas were optimized [130, 131]. As a result, a nanosecond Raman GFL was realized, generating single-mode radiation with an average power of 1.4 W at a wavelength of 4.42 μm [131] (Fig. 22b). This achievement convincingly demonstrated the capability of Raman GFLs to generate high average power (> 1 W), regardless of the large quantum defect of the conversion 1.56 → 4.42 μm, which converts 65% of energy into heat. The quantum efficiency of the Raman GFL, calculated from the average power, amounted to 53%, which corresponds to the theoretical limit, caused by optical losses (1.1 dB m^{-1}, $\lambda = 4.42$ μm) in a hollow-core optical fiber.

An all-fiber scheme of a hydrogen Raman GFL at a wavelength of 4.42 μm was realized in Ref. [132]. Using a standard optical fiber splicer, the fiber output of an erbium pump laser was spliced to the input face of the hollow-core fiber. The splice point ensured hermeticity and mechanical strength, and introduced optical losses of the order of 3 dB due to the difference between the mode field diameters of the spliced fibers. As a result, the all-fiber generation of nanosecond pulses with an average power of 360 mW at a wavelength of 4.42 μm was demonstrated. The quantum efficiency of the GFL amounted to 46%.

The lasing wavelength in Raman GFLs is easily changed by tuning the pump source wavelength. In Refs [133, 134], a hydrogen Raman GFL was implemented for monitoring the absorption bands of CO_2 molecules in the spectral region near 4.2 μm. For this purpose, the necessary wavelength of the erbium fiber pump laser was chosen in the region near 1.53 μm. By increasing the pump pulse duration to ~ 7 ns, the authors of [133] managed to decrease the influence of transient effects of the 1.53 → 4.2-μm Raman conversion in hydrogen and to reach quantum efficiency at a level of 74%. The energy of the output pulses reached 17.6 μJ. In addition, the studies of noise and long-term stability of the Raman GFL were carried out [134], which showed that the long-term drift of the energy and peak power is directly related to the large amount of heat released during the 1.53 → 4.2-μm Raman conversion. For practical application of Raman GFLs with a high average power, further investigation of long-term stability of their output parameters is necessary.

One of the advantages of Raman GFLs is the possibility of easy variation of the operating spectral range by merely changing the composition of the hollow core gas filling. For example, keeping the GFL design fully unchanged, including the hollow-core optical fiber and the erbium fiber pump laser, but using methane instead of hydrogen as the active gas, it is possible to implement single-cascade Raman GFL lasing in the spectral range near 2.84 μm [135, 136]. Moreover, by varying the erbium pump laser wavelength in the spectral range of 1.54–1.56 μm, continuous tuning of the Raman GFL lasing wavelength was demonstrated in the range from 2.796 to 2.863 μm [137].

To reach the lasing threshold in Raman GFLs, pump sources with sufficiently high radiation intensity are required. Such pump lasers are widely available in the spectral range near 1 μm and allow implementing several cascades of Raman conversion in hollow-core optical fibers. Using two segments of different hollow-core fibers filled with methane, the authors of Ref. [138] demonstrated two-cascade 1.06 → 1.54 → 2.81-μm Raman conversion. The pump pulses with a duration of 0.4 ns and a peak power of up to 400 kW were converted with the quantum efficiency of 87% and 75% in the first and the second cascade, respectively, so that the total quantum efficiency amounted to 65%.

Double-cascade Raman GFLs can also be implemented in a single segment of a hollow-core fiber, which was shown by the example of 1.06 → 1.54 → 2.81-μm conversion in methane [139, 140], where nearly 40% of pump quanta were converted into those with the wavelength of 2.81 μm. It was shown in [139] that the energy of output pulses at a wavelength of 2.81 μm can reach 113 μJ, and the estimated peak power exceeded ~ 10 MW. It is important to note that the pump pulse duration in Ref. [139] was only 12 ps, which is comparable to the phase relaxation time of an excited vibrational state in methane molecules and, therefore, can lead to a decrease in GFL efficiency because of the transient regime of Raman conversion. Although the duration of pulses at a wavelength of 2.81 μm was not studied in Ref. [139], the results of this work raise the question of the possibility of creating femtosecond GFLs of the mid-IR range.

Raman conversion of femtosecond pulses in hollow-core optical fibers filled with molecular gases faces the following problem. The duration of femtosecond pump pulses turns out to be much shorter than the phase relaxation time T_2 of the excited vibrational levels in molecular gases. For example, at a pressure of 30 atm, the phase relaxation time in molecular hydrogen amounts to $T_2 = 200$ ps, and in molecular deuterium $T_2 = 150$ ps [141]. Thus, for pump pulses with a duration less than ~ 10 ps, the Raman conversion in these gases occurs in a highly transient regime ($\tau_p \ll T_2$). As a result, in order to reach the threshold of stimulated Raman scattering, the pump intensity should be increased, which leads to manifestation of concurrent nonlinear effects based on Kerr nonlinearity, which can sufficiently reduce the efficiency of Raman conversion up to its complete suppression.

To solve this problem, a method based on introducing linear frequency modulation (chirp) into the pump pulses [142] is used. This method was demonstrated in bulk gas cells to generate ultrashort pulses in the visible and near-IR spectral ranges [143–148]. In recent years, this method was implemented in hollow-core optical fibers filled with various gases [149–153]. Under a pump at a wavelength of 1.03 μm, pulsed lasing was demonstrated with a duration of 560 fs at a wavelength of 1.46 μm in methane [149] and 39 fs at a wavelength of 1.8 μm in hydrogen [151]. Using a two-cascade conversion in deuterium [152] and in a mixture of deuterium and hydrogen [153], ultrashort pulses were generated in the mid-IR range. The measured duration of the output pulses amounted to 920 fs at a wavelength of 2.68 μm [152] and 4.6 ps at a wavelength of 3.9 μm [153].

It should be noted that the generation of ultrashort pulses in Raman GFLs not only is of interest in itself but can also be considered a step towards mid-IR supercontinuum generation in hollow-core optical fibers. In this case, the efficiency of converting the pump energy into the long-wave region increases thanks to the Raman mechanism. The possibility in principle of proceeding from the generation of fixed spectral components to the generation of a mid-IR supercontinuum using a Raman GFL was shown in our recent papers by both numerical simulation (up to 4 μm) [154] and experimentally (to 3.3 μm) [155] (Fig. 23).

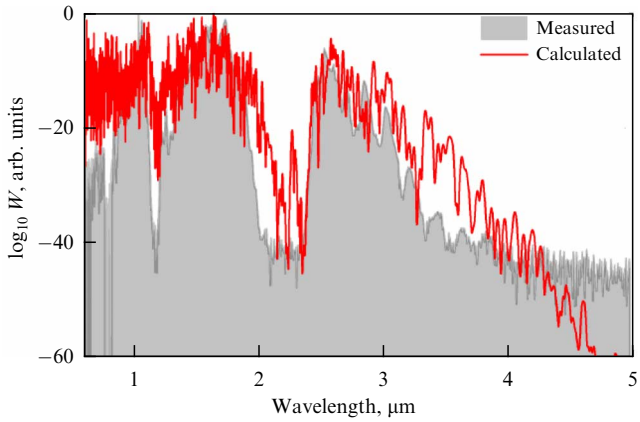

Figure 23. Output radiation spectrum of supercontinuum generation in a hollow-core fiber filled with molecular deuterium. Both the results of numerical simulation (red curve) and experimental data (grey filled curve) are shown. (Adopted from Ref. [155].)

Population inversion gas fiber lasers. The first optically pumped gas fiber laser with population inversion was demonstrated in 2010 [156, 157]. Laser generation was observed at two wavelengths near 3.1 μm in a hollow-core fiber filled with acetylene at a pressure of 9.3 mbar. An optical parametric oscillator served as a pump source. Its pulsed (5 ns) radiation was precisely tuned in the wavelength region near 1.52 μm to hit exactly the narrow (< 1 GHz) absorption lines of the active gas.

Acetylene was used as an active medium in many key experiments on the development of GFLs with population inversion; therefore, it is reasonable to consider the diagram of energy levels of acetylene in more detail. In the wavelength region near 1.53 μm, the acetylene molecule has an absorption band (Fig. 24a) corresponding to the transitions between the rotational sublevels of the ground and excited $(\nu_1 + \nu_3)$ vibrational states (Fig. 24b). The laser oscillations occur in the spectral region near 3.1 μm in the transitions between the $\nu_1 + \nu_3$ (the upper lasing level) and ν_1 (the lower lasing level) vibrational states. In this case, the dipole-allowed transitions are those with the change in rotational quantum number $\Delta j = \pm 1$, which leads to simultaneous lasing at two close wavelengths and is a characteristic feature of most GFLs based on the population inversion between the vibrational-rotational levels of molecular gases.

The radiative transitions from level ν_1 to the ground vibrational state are forbidden in the dipole approximation; therefore, for the relaxation of the lower lasing level population and restoration of the ground state population, it is necessary to provide a sufficient rate of molecular collisions determined by the active gas pressure. However, the molecular collisions cause the relaxation of not only the lower (ν_1) but also the upper $(\nu_1 + \nu_3)$ lasing level, which can lead to a decrease in efficiency or disruption of lasing. Thus, the choice of the active gas optimal pressure is of critical importance to obtain stable lasing, especially in the CW mode.

The lasing efficiency in the first acetylene GFL was only 1% [157]. As the pump pulse energy reached 1 μJ, the output pulses at a wavelength of 3.1 μm had an energy of 6 nJ and duration of ~ 4 ns. The efficiency was low because of the high level of optical losses (~ 20 dB m^{-1}) at the lasing wavelength in the hollow-core fiber, the length of which amounted to 1.65 m.

Decreasing the optical losses in the hollow-core fiber to 5 dB m^{-1} at a wavelength of 3.1 μm allowed an increase in the efficiency of nanosecond acetylene GFLs up to 27%, which is close the theoretical limit of efficiency for such lasers [158].

Further progress in GFLs is associated with the optimization of the optical pumping scheme. The fact that the absorption band of acetylene in the spectral region near 1.53 μm overlaps with the operating spectral range of erbium fiber lasers and amplifiers allowed using all-fiber sources of pumps instead of bulk parametric oscillators. The authors of Ref. [159] first pumped a GFL with a fiber-coupled tunable semiconductor laser, the radiation of which was modulated by an external modulator and then amplified by an erbium fiber amplifier. The obtained pump source generated pulses with a duration of 20 ns with a repetition rate of 10 kHz and maximum pulse energy of 5 μJ. The pump source wavelength was 1.53037 μm, coincident with one of the most intense absorption lines P(9) of acetylene molecules (see Fig. 24). It is important to note that the line width of the fiber pump source did not exceed 100 MHz, which is less than the spectral width of the P(9) absorption line (~ 500 MHz) and much less than the line width of the parametric oscillator (~ 3.5 GHz) used in earlier papers [157, 158]. As a result of more efficient absorption of pump photons, the ratio of the GFL output power to the *incident* pump power reached 20%, which is at least two times higher than in the earlier papers.

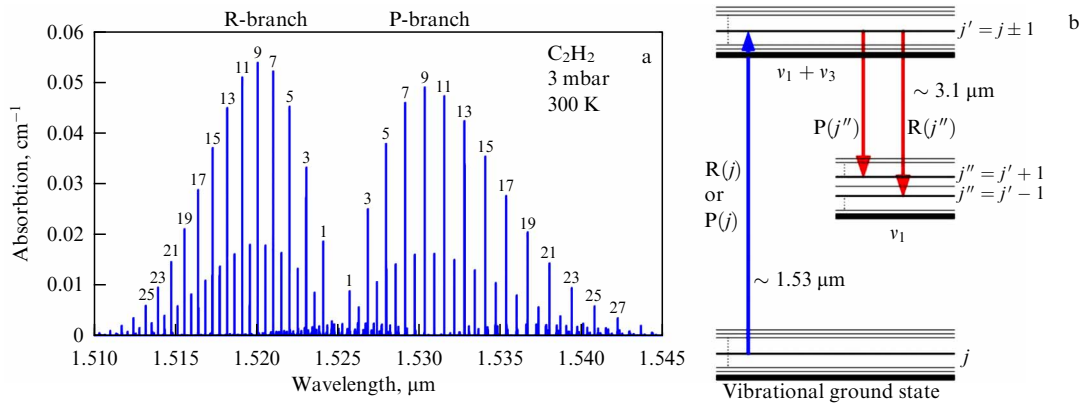

Figure 24. (a) Absorption spectrum of acetylene molecules in the wavelength region near 1.53 μm at a temperature of 300 K and pressure of 3 mbar. Spectrum is constructed using the HITRAN database. (b) Energy level diagram corresponding to vibrational-rotational states of the acetylene molecule participating in the formation of population inversion in the gas fiber laser.

In addition, to increase GFL efficiency, the active gas pressure in Ref. [159] was reduced to 0.7 bar, which led to a decrease in the rate of molecular collisions and substantially decreased the radiationless relaxation of the upper lasing level. As a result, the maximum GFL efficiency, calculated with respect to the *absorbed* pump power, amounted to 30% and the energy of the output pulses at a wavelength of ~ 3.1 μm reached 0.76 μJ [159]. It should be noted that the reduced concentration of the active gas molecules can lead to incomplete pump absorption and saturation of the gain. However, this problem was solved by using a longer hollow-core fiber (10.5 m), which was possible due to low optical losses (~ 0.1 dB m^{-1}) both at the pump wavelength (1.53 μm) and at the lasing wavelength (~ 3.1 μm) [159].

The intention to reduce the lasing threshold stimulated studies of GFL resonator designs. The authors of Ref. [160] applied an additional passive segment of a hollow-core fiber to recirculate the radiation generated at a wavelength of 3.1 μm in a ring resonator (Fig. 25). As a result, lowering the lasing threshold allowed the authors to demonstrate for the first time a mid-IR gas fiber laser operating in CW mode [160]. Moreover, when using an output mirror with a low transmission coefficient (7%), the lasing threshold decreased only to 16 mW, which allowed CW oscillation even while pumping the GFL with a diode laser with a power of 20 mW without using erbium fiber amplifiers.

Further studies have shown that the CW mode of acetylene GFL oscillation can also be obtained in a cavity-free single-pass setup [161]. Using a CW erbium fiber laser with an output power of 10 W as a pump source, stable CW oscillation of an acetylene GFL at a wavelength of 3.1 μm with an output power of 1.1 W and differential efficiency of 33% [161] was demonstrated, which approaches the theoretical limitations.

The possibilities of output power scaling in CW gas fiber lasers in the mid-IR range were considered in recent papers [162, 163]. The main idea of these papers consisted in increasing the pump wavelength so that it would be closer to the maximum of the gain contour of erbium amplifiers and still would overlap with the edge of the acetylene molecular absorption band (Fig. 24a). This allows increasing the output power of the erbium fiber pumping laser, at the same time decreasing the proportion of power contained in the broadband amplified spontaneous radiation, which does not participate in the excitation of active molecules but creates an additional thermal load on the input end face of the hollow-core fiber. The optimization of the erbium fiber pump source generating at a wavelength of 1.535 μm caused an increase in its output power to 50 W. The pump radiation was introduced into the hollow-core fiber filled with acetylene, the input face of which was placed in a low-pressure gas cell with water cooling. Under the continuous operation of the pump source, the output power of the GFL reached 6.5 W at a wavelength of 3.1 μm, and switching the pump to the pulsed mode (20 ns, 10 MHz) at the same average power (50 W) allowed demonstrating a record-breaking average power at a wavelength of 3.1 μm, reaching 7.9 W [163].

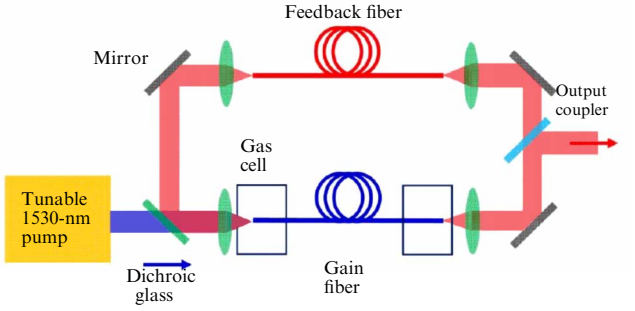

Figure 25. Schematic diagram of a GFL using a ring cavity [160].

Acetylene GFLs allow tuning the lasing wavelength, since the radiation of the erbium pump laser can be tuned over the spectrum, scanning different absorption lines of acetylene. Using this approach, a stepwise tuning of the lasing wavelength in the range of 3.09–3.21 μm with a step of ~ 4 nm has been demonstrated [164]. In this case, the mean output power of the GFL reached ~ 0.3 W in the pulsed mode and ~ 0.8 W in the CW mode.

Being a very convenient active medium, acetylene facilitated the fast development of gas fiber lasers. However, from the very first studies of GFLs based on population inversion, other molecular gases have also been studied as potential active media. In the spectral region near 3.1 μm, laser oscillation was demonstrated on HCN molecules [158] that have an energy level diagram analogous to that of acetylene.

The longest lasing wavelength reached in population inversion GFLs amounted to 4.6 μm when pumping at 1.517 μm and was obtained with N_2O molecules filling the hollow core of a fiber [165]. The differential efficiency of lasing was only 3%, limited by optical losses of ~ 30 dB m^{-1} at a wavelength of 4.6 μm in a hollow-core fiber. This result can be significantly improved, since hollow-core fibers in the mid-IR range with much less optical loss are now available.

Using CO_2 molecules as an active medium, in 2019, a gas fiber laser generating CW radiation at a wavelength of 4.3 μm was realized [166]. The pump source was a tunable laser diode, whose radiation was amplified with a thulium fiber amplifier. The pump wavelength was tuned to the absorption line R(30), corresponding to transitions of carbon dioxide molecules from the ground vibrational state to the $2\nu_1 + \nu_3$ (2.0006 μm) excited vibrational state. The lasing at a wavelength $\lambda = 4.3$ μm occurred on the transition between the upper $(2\nu_1 + \nu_3)$ and the lower $(2\nu_1)$ lasing energy levels. The optimal pressure of the active gas in the hollow core amounted to 5 mbar and the used hollow-core fiber 5 m in length had low optical losses at the wavelengths of both the pump (0.7 dB m^{-1}, $\lambda = 2$ μm) and the laser output (1.2 dB m^{-1}, $\lambda = 4.3$ μm). As a result, a slope efficiency of 19.3% with respect to the absorbed pump power was obtained, and the lasing output power at $\lambda = 4.3$ μm amounted to 82 mW, which at that time was the highest output power generated by any fiber laser at wavelengths above 4 μm. In subsequent papers, the author not only increased the GFL output power to ~ 560 mW but also demonstrated a stepwise tuning of the lasing wavelength within the spectral range of 4.27–4.43 μm [167].

HBr is one more molecular gas successfully used as a GFL active medium. The pump radiation from a thulium fiber laser with 8 W of power, tunable within a spectral range near 1.96 μm, was introduced into a 5-m-long hollow-core filled with HBr molecules at a pressure of 5 mbar. As a result, CW laser oscillation with stepwise wavelength tuning within the range of 3.81–4.496 μm was implemented [168]. The GFL output power reached 500 mW, the efficiency being about 18%. In subsequent papers, the HBr HGL output power was increased to 3.1 W at a wavelength of $\lambda = 4.16$ μm [169].

4.3 Studies of gas discharge fiber lasers

However, the characteristics of optically pumped GPLs are limited by the maximum characteristics of the pump laser. Full-scale realization of the capabilities of hollow-core fibers (resistance to high-intensity radiation, broad spectral range of transmission, etc.) in all-fiber optical circuits makes it necessary to solve the problem of generating the laser radiation in the HCF itself using no other solid-core fiber lasers with their inherent limitations as a pump source. One of the possible approaches to solving this problem is the development of gas discharge fiber lasers (GDFLs) based on hollow-core optical waveguides (although in the form of capillaries) was considered theoretically back in 1964 [10].

Today, gas discharge lasers are well known and widely used in research and technology (e.g., helium–neon and carbon dioxide lasers). The construction of a waveguide gas discharge laser (not yet in a fiber version) was first realized in 1971 as a helium–neon laser at 633 nm [170] and in 1972 as a CO_2 laser [171]. Note also the demonstration of a waveguide helium–neon laser at 3.39 μm in 1975 [172]. In all these cases, the generated radiation was guided inside glass capillaries with inner diameters of 3.3 mm [171], 430 μm [170], and 510 μm [172]. Decreasing the waveguide diameter facilitates reducing the bending optical losses. In addition, the decrease in the diameter of the discharge tube usually leads to the growth of optical gain in the gas discharge plasma. But already at a capillary inner diameter as small as about 0.5 mm, researchers faced electric discharge instability, and further reduction of the capillary diameter made maintaining the discharge rather problematic due to the large loss of electrons on the capillary walls. In a few papers, this effect was overcome using a combined electric pump. Thus, pumping in the form of a combination of DC voltage and radio frequency voltage was used in Ref. [170] and a combination of DC and microwave voltage in Ref. [172]. As a result, rigid capillary waveguide lasers are still being exploited, but the use of capillaries as waveguides and the requirement of rectilinearity that follows (needed to ensure a low level of optical losses [10]) commonly restrict their length to a few tens of centimeters.

The possibility of creating fiber gas discharge lasers began to be investigated nearly 15 years ago, soon after the invention of hollow-core fibers. The main problem here is the difficulty of maintaining plasma in the thin (about 100 μm in diameter) hollow core. This order of the diameter value is used practically in all studies of HCFs and is determined by the acceptable level of HCF bending losses. The first studies on the way to creating GDFLs were carried out at the Hong Kong Polytechnic University in 2007–2008 [173–175]. In these studies, the discharge was excited in an HCF by applying a DC voltage of $\sim$ 10 kV, both in glass capillaries and in HCFs with various values of the inner diameter (for capillaries) and diameters of the hollow core (for HCFs). In terms of exciting the electric discharge, there is no difference between a usual capillary and an HCF with similar holes. It should also be noted that a conventional glass capillary in fact is also an optical waveguide with a hollow core (as was shown in Ref. [10]). In these papers, it turned out to be possible to demonstrate the ignition and maintenance of a discharge in glass capillaries and HCFs with the inner diameter $d_C = 344$, 250, 150, 50, and 20 μm in Ar, He, and CO_2 at a pressure of about 20 Torr. The lengths of waveguide segments between the electrodes were very small, from 13 to 2.9 cm. When using higher voltages ($\sim$ 30 kV), it was possible to excite the discharge in a segment of an optical fiber with the hollow core diameter of 250 μm and length of 26 cm [175].

The next series of studies on GDFLs with the excitation of electric discharge by DC voltage was carried out at the University of Bath (United Kingdom) [176–179]. Already in 2014, the optical gain in an electrically pumped gas-filled HCF was reported [176]. A DC electric charge with a voltage up to 40 kV was used for pumping. The mixture of He and Xe in the proportion of 5:1 at a total pressure of $\sim$ 10 Torr was used. The hollow core diameter of the revolver-type HCF was $d_C = 120$ μm. With a 100% reflecting mirror at one end of the fiber, the level of luminescence at the output at the other end of the fiber increased more than twofold, which was interpreted by the authors as the amplification of radiation by the atomic transition of Xe. The gain was recorded in this way at the transitions of neutral xenon atoms with wavelengths of 3.11, 3.37, and 3.51 μm. However, no GDFL was created, and this result has not been further developed to date.

Finally, in several studies carried out by the team of Prof. Benabid of the University of Limoges (France), the possibilities of exciting an electric discharge in hollow-core optical fibers by electromagnetic radiation in the microwave range were investigated (see review [6]). Indeed, in terms of several parameters, methods with gas lasers excited by a microwave discharge can have a substantial advantage over excitation by DC voltage or by high frequency (HF) fields [180]. In papers by the Benabid team, the possibility was shown of igniting and maintaining electric discharge in a hollow-core fiber with the $d_C = 125$ μm core filled with argon [181] under the action of a microwave field source with a frequency of 2.45 GHz and power of 200 W. The discharge was maintained in the fiber hollow core at the expense of exciting a surface electromagnetic wave propagating along the plasma column filling the core of the HCF. A surface electromagnetic wave was formed using a special surfatron device [6], comprising a cavity for the microwave radiation. As was demonstrated earlier [182], such a device is capable of efficient excitation of the microwave discharge in tubes with a large diameter ($\sim$ 1 cm). The length of the HFC region occupied by the discharge plasma was restricted to a value of $\sim$ 4 cm. The argon pressure was about 1 Torr. So far, no optical gain has been observed in such a device, but it was proposed to be used as a source of UV radiation.

An analysis of the above papers allows the following conclusions. Using DC voltage to excite an electric discharge in an HCF with a hollow core diameter of the order of 100 μm requires high voltage values (tens of kV), which substantially restricts the possibilities of applying such devices. In addition, the use of DC voltage is accompanied by the necessity to place the electrodes inside the gas volume of the GDFL, increasing the probability of violating the waveguide properties of the fiber hollow core by the particles produced in the process of electrode degradation during operation.

The use of radiofrequency fields eliminates the need for electrodes, but otherwise differs little from the use of DC voltage [77]. Moreover, generating the necessary values of field strength in the radiofrequency range is much more difficult than in the case of DC voltage or in the microwave range.

Using electromagnetic waves in the microwave range, in particular, at frequencies of the order of 3 GHz, to maintain the discharge makes the amplitude of electron vibration in the field of the same order as or smaller than the hollow core diameter, which reduces the probability of electron

loss on the fiber wall as compared to the lower-frequency fields. Moreover, the wide use of magnetrons operating at a frequency of 2.45 GHz in domestic appliances (popular microwave ovens) made the sources of this radiation relatively cheap and easily available.

The possibility of maintaining a discharge in inert gases in HCFs with a hollow core diameter of 100 μm or more by means of microwave radiation has been shown experimentally in Ref. [183]. The electric field strengths necessary to maintain the microwave discharge in hollow cores of various diameters filled with various inert gases at various pressures were experimentally measured in Ref. [184]. The obtained results lay the foundation for the creation of the first gas discharge fiber laser.

4.4 First gas discharge fiber laser

To deliver microwave radiation to the middle of the fiber core, a side input design with the electric field vector directed perpendicular to the HCF axis was chosen. An evident advantage of this scheme is the absence of the necessity to use high voltages (tens of kilovolts) to maintain the discharge.

4.4.1 Setup of the experiment. A magnetron operating at a frequency of $\nu = 2.45$ GHz in the pulsed mode was used as a microwave field source to maintain the gas discharge in the experiments. The pulse repetition rate amounted to ~ 400 Hz, the pulse duration was ~ 20 μs, and the maximum peak power reached 8 kW.

Magnetron radiation was introduced into the waveguide, which was single-mode for the magnetron radiation, and only the H_{10} wave propagated through it. The transverse dimensions of the waveguide were too large compared to the hollow core diameter for efficient absorption of the microwave field energy by the plasma in the hollow core of the fiber.

Therefore, for a kind of focusing of microwave radiation, a slot antenna setup was used (Fig. 26). A more detailed description of exciting the microwave discharge in an HCF can be found in Ref. [183].

Experiments were carried out with HCFs made of pure fused silica (F300, Heraeus) filled with inert gases (argon, neon, helium at a pressure from units to hundreds of Torrs); the diameter of the fiber hollow core sequentially decreased to 100 μm.

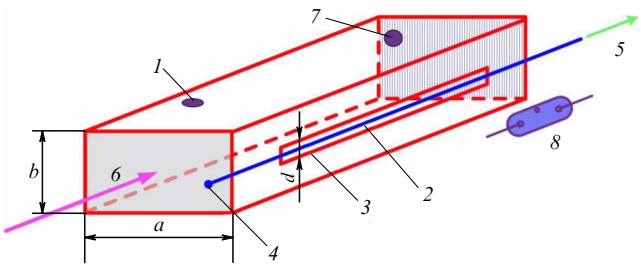

Figure 26. Schematic diagram of the experiment: *1* — part of rectangular microwave waveguide, $a = 9$ cm, $b = 4.5$ cm, *2* — hollow-core optical fiber, *3* — longitudinal slot in the side wall of the waveguide, *4* — sealed end of the optical fiber; *5* — connection of the optical fiber to the vacuum system and gas filling system, *6* — direction of propagation of electromagnetic radiation from magnetron along the waveguide, *7* — piston reflecting radiation back and thus forming a standing wave; *8* — mercury lamp for initiating microwave discharge.

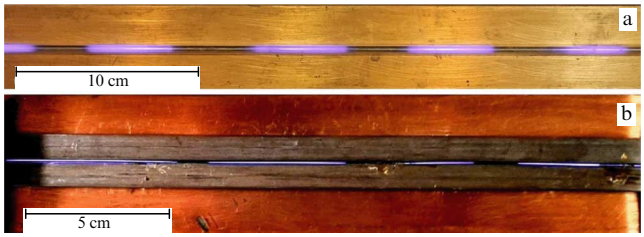

Figure 27. Microwave discharge in a simple capillary (a) and in a revolver optical fiber (b) filled with argon at a pressure of 20 Torr against the background of the side surface of the waveguide with the slot in the middle. Capillary with inner diameter of 3 mm is placed directly into the slot on the side surface of the waveguide; ROF with hollow core diameter of 230 μm is placed between special pads to reduce effective width of the slot. In the microwave waveguide, a standing wave was formed due to the interference of the incident wave and the wave reflected from a short-circuiting piston. Quality of the interference pattern depended on the parameters of piston adjustment.

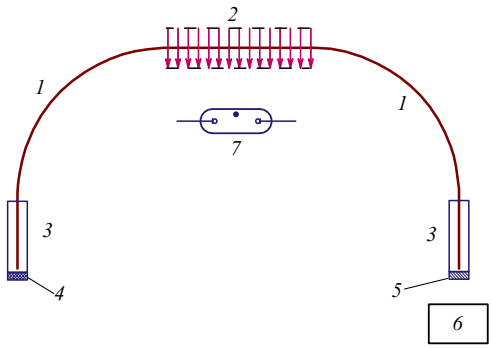

Figure 28. Schematic diagram of the experiment: *1* — revolver HCF 120 cm long; *2* — microwave field region 32 cm long; *3* — miniature vacuum chambers connected to the gas-filling system; *4* — nontransmitting laser mirror; *5* — output laser mirror; *6* — recording instrumentation (photodetector, spectrum analyzer); *7* — mercury lamp for initiating microwave discharge.

It is known that the ignition (or initiation) of discharges of all types (including those under the action of a microwave field) requires much higher electric field magnitudes than its maintenance after the initiation. Therefore, in Ref. [183], the preliminary ionization of the gas by means of UV radiation was used to initiate the electric discharge in the HCF under the action of a microwave field. As a result, the electric discharge was ignited and maintained by the microwave field in the entire segment of the HCF, located in a slot on the side surface of the microwave waveguide, i.e., at a length of around 300 mm.

A typical photograph of the optical fiber with the discharge burning in it is presented in Fig. 27.

4.4.2 Gas discharge xenon laser based on a hollow-core optical fiber. The method of exciting a gas discharge in an HCF exposed to microwave radiation allowed the first demonstration of a GDFL on a revolver hollow-core optical fiber [185].

A schematic diagram of the GDFL is presented in Fig. 28. The revolver fiber was filled with an He:Ar:Xe mixture of gases in the proportion of 100:10:1 at a total pressure of 130 Torr. The fiber ends were hermetically inserted into miniature vacuum chambers connected to a vacuum system and a system of gas filling. The design of the vacuum

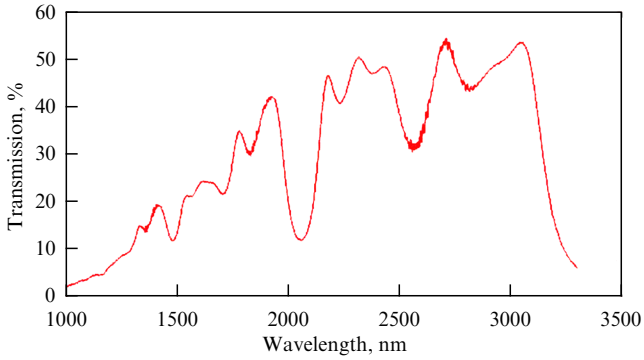

Figure 29. Transmission spectrum of the output laser mirror (*5* in Fig. 28).

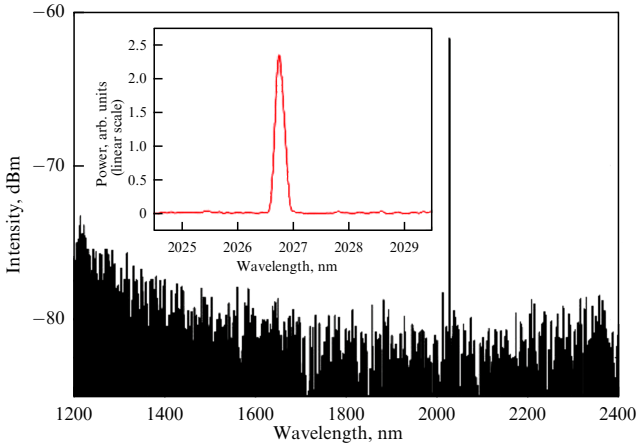

Figure 31. Radiation spectrum of a xenon gas discharge fiber laser.

chambers also comprised laser cavity mirrors and allowed their alignment. High-reflection mirror *4* (see Fig. 28) of the cavity was a polished aluminum plate. Output mirror *5* had a multilayer coating that provided a high reflection coefficient at the possible emission lines of the xenon laser. The transmission spectrum of the output mirror is presented in Fig. 29. A part of the laser revolver fiber 32 cm long was placed in the region of the pulsed microwave field at a frequency of 2.45 GHz with a pulse duration of 20 μs and pulse repetition rate of 400 Hz. The maximum microwave electric field strength directed perpendicular to the fiber axis reached ~ 1 kV cm^{-1} in the experiments. A view of the revolver HCF cross section is shown in Fig. 30b. The hollow core had a diameter of 130 μm.

Microwave discharge was initiated in the HCF by means of a short-term (~ 1 s) exposure to UV radiation from a mercury lamp (*7*) (see Fig. 28). After alignment of the mirrors, laser oscillations arose at a wavelength of 2.027 μm. The laser radiation spectrum was recorded with a Yokogawa AQ637B spectrum analyzer (Fig. 31). Preliminarily, the lasing line position was determined by means of a photodetector sensitive in the spectral range from 1 to 5 μm (Fig. 30a). The maximum lasing peak power was ~ 1 mW.

The results presented show a possibility in principle of creating a new type of laser — a gas discharge fiber laser. This opens up the possibility of improving the design of such lasers in the process of further investigations. In the future, GDFLs that combine the advantages of fiber and gas discharge lasers will find numerous applications in various areas of science and technology.

5. Conclusion

Hollow-core optical fibers opened fundamentally new capabilities of transmission, generation, and nonlinear conversion of optical radiation in such regimes, which are not available for solid-core fibers. The invention of hollow-core revolver-type optical fiber was an important milestone on the way of HCF development. Revolver fibers are distinct from

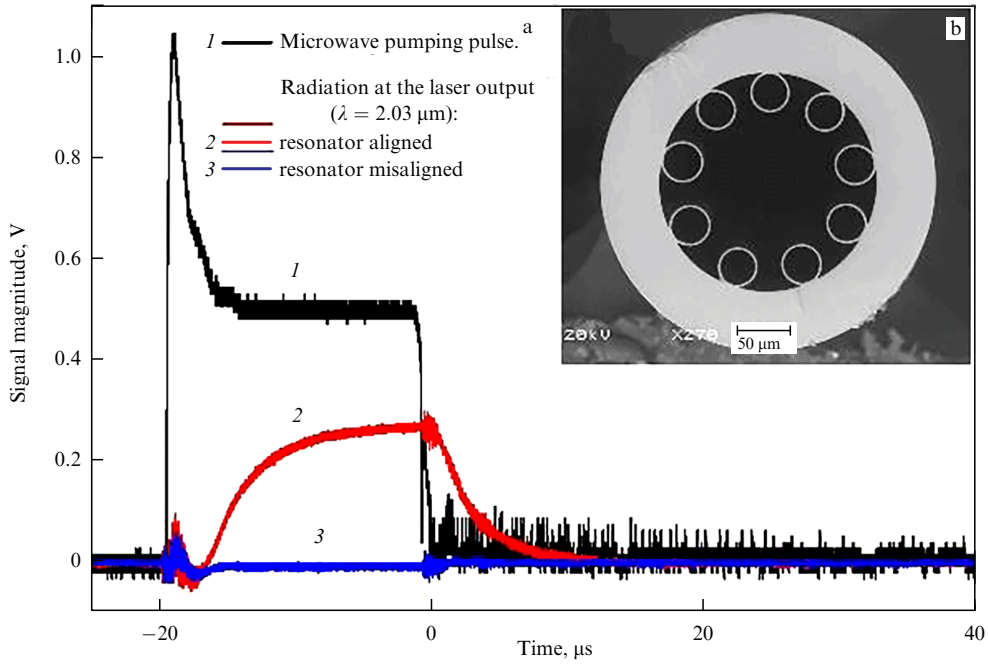

Figure 30. (a) Oscillograms of the microwave pumping pulse and radiation of a xenon GDFL under various conditions. (b) Cross section of the revolver HCF with which the GDFL oscillation was obtained.

other types of HCFs by their design simplicity, predictability, and reproducibility of optical properties. These properties not only opened access to studying these optical fibers for many research groups but also made revolver fibers a starting point for developing new designs of hollow-core optical fibers with increasingly perfect characteristics.

Practically all hollow-core optical fibers that presently find application in research and technology are those with reflective cladding formed by a single layer of capillaries not in contact with each other, i.e., hollow-core revolver-type optical fibers. The best characteristics are possessed by those hollow-core optical fibers with one layer of nested capillaries, often referred to as NANFs (nested anti-resonant nodeless fibers) and DNANFs (double NANFs). They are exactly those that presently demonstrate the lowest optical losses. However, the anti-resonant mechanism of loss reduction in HCFs alone is insufficient to provide the loss level obtained in such fibers. The performed calculations of the electromagnetic field in revolver fibers show that a substantial contribution to the reduction of leaky losses is due to the negative curvature of the boundary between the cladding and the core.

To date, the hollow-core optical fibers have already manifested their unique properties for the implementation of new communication lines, nonlinear devices and radiation generators, the transmission of high-power radiation in various frequency ranges, and the development of new types of fiber lasers, including gas discharge ones.

Further development of hollow-core fibers and devices based on them will surely make a great contribution to solving many problems, from creating a new generation of high-speed optical communication systems to the development of new types of sensors, sources, and converters of optical radiation with the unique properties required for numerous practical applications.

The study was funded by the Russian Scientific Foundation, grants 22-22-00575, https://rscf.ru/project/22-22-00575/ (theoretical studies and numerical experiments) and 19-12-00361, https://rscf.ru/project/10-12-00361/ (fabricating technology, experimental investigation, and application of hollow-core optical fibers).

References

1. Gregan R F et al. *Science* **285** 1537 (1999)
2. Pryamikov A D et al. *Opt. Express* **19** 1441 (2011)
3. Wang Y Y et al. *Opt. Lett.* **36** 669 (2011)
4. Kolyadin A N et al. *Opt. Express* **21** 9514 (2013)
5. Fokoua E N et al. *Adv. Opt. Photon.* **15** 1 (2023)
6. Debord B et al. *Fibers* **7** (2) 16 (2019)
7. Bufetov I A et al. *Fibers* **6** (2) 39 (2018)
8. Markos C et al. *Rev. Mod. Phys.* **89** 045003 (2017)
9. Wei C et al. *Adv. Opt. Photon.* **9** 504 (2017)
10. Marcatili E A J, Schmeltzer R A *Bell Syst. Tech. J.* **43** 1783 (1964)
11. Miyagi M, Nishida S *IEEE Trans. Microwave Theory Tech.* **28** 536 (1980)
12. Duguay M A et al. *Appl. Phys. Lett.* **49** 13 (1986)
13. Croitoru N et al. *Fiber Integr. Opt.* **6** 347 (1987)
14. Wilson S, Jenkins R, Devereux R *IEEE J. Quantum Electron.* **23** 52 (1987)
15. Harrington J A *Fiber Integr. Opt.* **19** 211 (2000)
16. Birks T A et al. *Electron. Lett.* **31** 1941 (1995)
17. Benabid F, Roberts P J *J. Mod. Opt.* **58** 87 (2011)
18. Roberts P J et al. *Opt. Express* **13** 236 (2005)
19. Shephard J D et al. *Opt. Express* **13** 7139 (2005)
20. Wheeler N V et al. *Opt. Lett.* **39** 295 (2014)
21. Couny F et al. *Science* **318** 1118 (2007)
22. Ghenuche P et al. *Opt. Lett.* **37** 4371 (2012)
23. Temelkuran B et al. *Nature* **420** 650 (2002)
24. Yu F, Knight J C *Opt. Express* **21** 21466 (2013)
25. Belardi W, Knight J C *Opt. Lett.* **39** 1853 (2014)
26. Poletti F *Opt. Express* **22** 23807 (2014)
27. Kosolapov A F et al. *Quantum Electron.* **46** 267 (2016); *Kvantovaya Elektron.* **46** 267 (2016)
28. Debord B et al. *Optica* **4** 209 (2017)
29. Litchinitser N M et al. *Opt. Lett.* **27** 1592 (2002)
30. Pryamikov A *Photonics* **10** 1035 (2023)
31. Pryamikov A D et al. *Sci. Rep.* **10** 2507 (2020)
32. Denisov A N et al. *Quantum Electron.* **46** 1031 (2016); *Kvantovaya Elektron.* **46** 1031 (2016)
33. Ebendorff-Heidepriem H, Monro T M *Opt. Express* **15** 15086 (2007)
34. Cook K et al. *Opt. Lett.* **40** 3966 (2015)
35. Chu Y et al. *Opt. Lett.* **44** 5358 (2019)
36. Luo Y et al. *Opt. Fiber Technol.* **58** 102299 (2020)
37. Yu F, Wadsworth W J, Knight J C *Opt. Express* **20** 11153 (2012)
38. Gao S, Wang Y, Wang P, in *2017 Conf. on Lasers and Electro-Optics Pacific Rim* (Washington, DC: Optica Publ. Group, 2017) paper s2024
39. Klimczak M et al., in *Conf. on Lasers and Electro-Optics* (OSA Technical Digest) (Washington, DC: Optica Publ. Group, 2019) paper STh1L.5, https://doi.org/10.1364/CLEO_SI.2019.STh1L.5
40. Poulain M, Poulain M, Lucas J *Mater. Res. Bull.* **10** (4) 243 (1975)
41. Li Y et al. *Opt. Mater.* **96** 109281 (2019)
42. Jiang X et al., in *Conf. on Lasers and Electro-Optics* (OSA Technical Digest) (Washington, DC: Optica Publ. Group, 2016) paper AM3J.4, online, https://doi.org/10.1364/CLEO_AT.2016.AM3J.4
43. Gong Z et al. *J. Opt.* **23** 115005 (2021)
44. Désévédavy F et al. *Opt. Mater.* **32** 1532 (2010)
45. Hu M et al. *Opt. Laser Technol.* **158** (Pt. B) 108932 (2023)
46. Dorofeev V V et al. *J. Non-Cryst. Solids* **357** 2366 (2011)
47. Dorofeev V V et al. *Opt. Mater.* **33** 1911 (2011)
48. Ventura A et al. *Opt. Express* **28** 16542 (2020)
49. Gattass R R et al. *Opt. Express* **24** 25697 (2016)
50. Wang Y Y et al., in *Conf. on Lasers and Electro-Optics 2010* (OSA Technical Digest) (Washington, DC: Optica Publ. Group, 2010) paper CPDB4, CD, https://doi.org/10.1364/CLEO.2010.CPDB4
51. Gao S et al. *Nat. Commun.* **9** 2828 (2018)
52. Amrani F et al. *Light Sci. Appl.* **10** 7 (2021)
53. Jasion G T et al., in *Optical Fiber Communication Conf., OFC 2022* (Technical Digest Series, Eds S Matsuo et al.) (Washington, DC: Optica Publ. Group, 2022) paper Th4C.7, https://doi.org/10.1364/OFC.2022.Th4C.7
54. Yu F et al. *Opt. Express* **26** 10879 (2018)
55. Osório J H et al., in *Conf. on Lasers and Electro-Optics* (Technical Digest Series) (Washington, DC: Optica Publ. Group, 2022) paper SW4K.6, https://doi.org/10.1364/CLEO_SI.2022.SW4K.6
56. Zhang X et al. *Opt. Lett.* **47** 589 (2022)
57. Wheeler N V et al. *Opt. Lett.* **42** 2571 (2017)
58. Yu F et al. *APL Photon.* **4** 080803 (2019)
59. Davidson I A et al., in *OSA Advanced Photonics Congress, AP, 2020, IPR, NP, NOMA, Networks, PVLED, PSC, SPPCom, SOF, AP, 2020* (OSA Technical Digest, Eds L Caspani et al.) (Washington, DC: Optica Publ. Group, 2020) paper SoW1H.7
60. Bradley T D et al., in *2018 European Conference on Optical Communication, ECOC, Rome, Italy, 23–27 September 2018* (Piscataway, NJ: IEEE, 2018) paper Th3F.2, https://doi.org/10.1109/ECOC.2018.8535324
61. Bradley T D et al., in *45th European Conf. on Optical Communication, ECOC 2019, Dublin, Ireland, 22–26 September 2019* (Piscataway, NJ: IEEE, 2019) paper Th3F.1, https://doi.org/10.1049/cp.2019.1028
62. Jasion G T et al. *Optical Fiber Communication Conf. Postdeadline Papers 2020* (Washington, DC: Optica Publ. Group, 2020) paper Th4B.4, https://doi.org/10.1364/OFC.2020.Th4B.4
63. Sakr H et al., in *Optical Fiber Communication Conf., OFC, 2021* (OSA Technical Digest, Eds P Dong et al.) (Washington, DC: Optica Publ. Group, 2021) paper F3A.4, https://doi.org/10.1364/OFC.2021.F3A.4
64. Hong Y et al. *J. Lightwave Technol.* **38** 2849 (2020)
65. Sakr H et al. *J. Lightwave Technol.* **38** 159 (2020)
66. Nespola A et al. *J. Lightwave Technol.* **39** 813 (2021)

67. Poggiolini P, Poletti F *J. Lightwave Technol.* **40** 1605 (2022)
68. Saljoghei A et al., arXiv:2106.05343
69. Dianov E M et al. *Electron. Lett.* **38** 783 (2002)
70. Biriukov A S, Dianov E M *Proc. SPIE* **4083** 81 (2000)
71. Bobkov K et al. *Opt. Express* **29** 1722 (2021)
72. Smith A V et al. *IEEE J. Sel. Top. Quantum Electron.* **15** 153 (2009)
73. Mulvad H C H et al. *Nat. Photon.* **16** 448 (2022)
74. Cooper M A et al. *Optica* **10** 1253 (2023); https://preprints.opticaopen.org/ndownloader/files/40858583
75. Couairon A, Mysyrowicz A *Phys. Rep.* **441** 47 (2007)
76. Eilzer S, Wedel B *Fibers* **6** (4) 80 (2018)
77. Raizer Yu P *Gas Discharge Physics* (Berlin: Springer-Verlag, 1991); Translated from Russian: *Fizika Gazovogo Razryada* (Moscow: Nauka, 1987)
78. Bufetov I A et al. *Opt. Express* **27** 18296 (2019)
79. Kashyap R *Opt. Express* **21** 6422 (2013)
80. Raizer Yu P *Laser-Induced Discharge Phenomena* (New York: Consultants Bureau, 1977); Translated from Russian: *Lazernaya Iskra i Rasprostranenie Razryadov* (Moscow: Nauka, 1974)
81. Bufetov I A, Dianov E M *Phys. Usp.* **48** 91 (2005); *Usp. Fiz. Nauk* **175** 100 (2005)
82. Dianov E M et al. *JETP Lett.* **83** 75 (2006); *Pis'ma Zh. Eksp. Teor. Fiz.* **83** 84 (2006)
83. Dianov E M, Bufetov E M, Frolov A A *J. Opt.* **33** 171 (2004)
84. Kolyadin A N, Kosolapov A F, Bufetov I A *Quantum Electron.* **48** 1138 (2018); *Kvantovaya Elektron.* **48** 1138 (2018)
85. Kolyadin A N et al. *Prikl. Fotonika* **6** (3–4) 171 (2019)
86. Bufetov I A et al. *Quantum Electron.* **38** 441 (2008); *Kvantovaya Elektron.* **38** 441 (2008)
87. Bufetov I A, Fedorov V B, Fomin V K *Combust. Explos. Shock Waves* **22** 274 (1986); *Fiz. Goren. Vzryva* (3) 18 (1986)
88. Tauer J et al. *Laser Phys. Lett.* **4** 444 (2007)
89. Dumitrache C, Rath J, Yalin A P *Materials* **7** 5700 (2014)
90. Krylov A A et al. *Quantum Electron.* **48** 589 (2018); *Kvantovaya Elektron.* **48** 589 (2018)
91. Frolov A A et al. *Proc. SPIE* **6193** 61930W (2006)
92. Bufetov I "Optical discharge propagation along hollow-core fiber", media posted on 2019-06-14, https://opticapublishing.figshare.com/articles/media/Visualization1_mp4/8057399
93. "Christmas with Fiber Fuse", Materials Revealed! National Institute for Materials Science (NIMS), https://www.youtube.com/watch?v=0yq0GoH0TH8
94. Ramsden S A, Savic P *Nature* **203** 1217 (1964)
95. Sedov L I *Similarity and Dimensional Methods in Mechanics* (Moscow: Mir Publ., 1982); Translated from Russian: *Metody Podobiya i Razmernosti v Mekhanike* 9th ed. rev. (Moscow: Nauka, 1981); Translated into English from 10th updated Russian ed.: *Similarity and Dimensional Methods in Mechanics* (Boca Raton, FL: CRC Press, 1993)
96. Nisoli M, De Silvestri S, Svelto O *Appl. Phys. Lett.* **68** 2793 (1996)
97. Nagy T, Simon P, Veisz L *Adv. Phys. X* **6** 1845795 (2021)
98. Agrawal G P *Nonlinear Fiber Optics* 5th ed. (Amsterdam: Elsevier. Academic Press, 2013)
99. Nisoli M et al. *Opt. Lett.* **22** 522 (1997)
100. Gerullo G et al. *IEEE J. Sel. Top. Quantum Electron.* **6** 948 (2000)
101. Li C et al. *Opt. Express* **22** 1143 (2014)
102. Qian J et al. *Photonics Res.* **9** 477 (2021)
103. Andriukaitis G et al. *Opt. Lett.* **36** 1914 (2011)
104. Nagy T, Forster M, Simon P *Appl. Opt.* **47** 3264 (2008)
105. Böhle F et al. *Laser Phys. Lett.* **11** 095401 (2014)
106. Heckl O H et al. *Opt. Express* **19** 19142 (2011)
107. Guichard F et al. *Opt. Express* **23** 7416 (2015)
108. Köttig F et al. *Optica* **4** 1272 (2017)
109. Köttig F et al. *Opt. Express* **28** 9099 (2020)
110. Losev L et al. *Fibers* **11** (2) 22 (2023)
111. Murari K et al. *Optica* **3** 816 (2016)
112. Murari K et al. *Photonics Res.* **10** 637 (2022)
113. Wagner N L et al. *Phys. Rev. Lett.* **93** 173902 (2004)
114. Im S-J, Husakou A, Herrmann J *Opt. Express* **17** 13050 (2009)
115. Joly N Y et al. *Phys. Rev. Lett.* **106** 203901 (2011)
116. Ermolov A et al. *Opt. Lett.* **44** 5005 (2019)
117. Balciunas T et al. *Nat. Commun.* **6** 6117 (2015)
118. Luan J, Russell P St J, Novoa D *Opt. Express* **29** 13787 (2021)
119. Travers J C et al. *Nat. Photon.* **13** 547 (2019)
120. Ermolov A et al. *Phys. Rev. A* **92** 033821 (2015)
121. Sollapur R et al. *Light Sci. Appl.* **6** e17124 (2017)
122. Yatsenko Yu P et al. *Quantum Electron.* **47** 553 (2017); *Kvantovaya Elektron.* **47** 553 (2017)
123. Adamu A I et al. *Sci. Rep.* **9** 4446 (2019)
124. Gao S-F et al. *Laser Photon. Rev.* **16** 2100426 (2022)
125. Benabid F et al. *Science* **298** 399 (2002)
126. Benabid F et al. *Phys. Rev. Lett.* **93** 123903 (2004)
127. Gladyshev A V et al., in *Conf. on Lasers and Electro-Optics* (OSA Technical Digest) (Washington, DC: Optica Publ. Group, 2017) paper STu1K.2, https://doi.org/10.1364/CLEO_SI.2017.STu1K.2, online
128. Gladyshev A V et al. *IEEE J. Sel. Top. Quantum Electron.* **24** 0903008 (2018)
129. Gladyshev A V et al. *Quantum Electron.* **47** 491 (2017); *Kvantovaya Elektron.* **47** 491 (2017)
130. Gladyshev A V et al. *Quantum Electron.* **47** 1078 (2017); *Kvantovaya Elektron.* **47** 1078 (2017)
131. Astapovich M S et al. *IEEE Photon. Technol. Lett.* **31** 78 (2019)
132. Gladyshev A V et al., in *2019 Conf. on Lasers and Electro-Optics Europe and European Quantum Electronics Conf.* (OSA Technical Digest) (Washington, DC: Optica Publ. Group, 2019) paper cj_3_3
133. Wang Y et al. *Opt. Lett.* **45** 1938 (2020)
134. Wang Y et al. *J. Lightwave Technol.* **39** 3560 (2021)
135. Krylov A A et al. *Quantum Electron.* **52** 274 (2022); *Kvantovaya Elektron.* **52** 274 (2022)
136. Krylov A A et al. *Quantum Electron.* **52** 685 (2022); *Kvantovaya Elektron.* **52** 685 (2022)
137. Huang W et al. *Laser Phys. Lett.* **16** 085107 (2019)
138. Li Z et al. *Opt. Lett.* **43** 4671 (2018)
139. Cao L et al. *Opt. Express* **26** 5609 (2018)
140. Zhang X et al. *IEEE Photon. Technol. Lett.* **34** 1007 (2022)
141. Hanna D, Pointer D, Pratt D *IEEE J. Quantum Electron.* **22** 332 (1986)
142. Jordan C et al. *Appl. Phys. B* **59** 471 (1994)
143. Konyashchenko A V, Losev L L, Tenyakov S Yu *Opt. Express* **15** 11855 (2007)
144. Didenko N V et al. *Quantum Electron.* **45** 1101 (2015); *Kvantovaya Elektron.* **45** 1101 (2015)
145. Vicario C et al. *Opt. Lett.* **41** 4719 (2016)
146. Konyashchenko A V et al. *Quantum Electron.* **47** 593 (2017); *Kvantovaya Elektron.* **47** 593 (2017)
147. Konyashchenko A V, Losev L L, Pazyuk V S *Opt. Lett.* **44** 1646 (2019)
148. Didenko N V, Konyashchenko A V, Losev L L *Quantum Electron.* **50** 834 (2020); *Kvantovaya Elektron.* **50** 834 (2020)
149. Gladyshev A V et al. *Quantum Electron.* **49** 1089 (2019); *Kvantovaya Elektron.* **49** 1089 (2019)
150. Kergoustin D et al., in *2019 Conf. on Lasers and Electro-Optics Europe and European Quantum Electronics Conf.* (OSA Technical Digest) (Washington, DC: Optica Publ. Group, 2019) paper cd_3_5
151. Loranger S, Russell P St J, Novoa D *J. Opt. Soc. Am. B* **37** 3550 (2020)
152. Gladyshev A V et al. *Opt. Mater. Express* **10** 3081 (2020)
153. Gladyshev A V et al. *Optoelectron. Instrum. Data Proces.* **59** 10 (2023); *Avtometriya* **59** (1) 15 (2023)
154. Yatsenko Yu P, Gladyshev A V, Bufetov I A *Quantum Electron.* **51** 1068 (2021); *Kvantovaya Elektron.* **51** 1068 (2021)
155. Gladyshev A et al. *Photonics* **9** 997 (2022)
156. Vasudevan Nampoothiri A V et al. *Proc. SPIE* **7580** 758001 (2010)
157. Jones A M et al. *Opt. Express* **19** 2309 (2011)
158. Vasudevan Nampoothiri A V et al. *Opt. Mater. Express* **2** 948 (2012)
159. Wang Z et al. *Opt. Express* **22** 21872 (2014)
160. Abu Hassan M R et al. *Optica* **3** 218 (2016)
161. Xu M, Yu F, Knight J *Opt. Lett.* **42** 4055 (2017)
162. Huang W et al. *Opt. Laser Technol.* **151** 108090 (2022)
163. Huang W et al. *Opt. Lett.* **47** 2354 (2022)
164. Zhou Z et al. *Opt. Express* **26** 19144 (2018)
165. Aghbolagh F B A et al. *Opt. Lett.* **44** 383 (2019)
166. Cui Y et al. *Optica* **6** 951 (2019)
167. Cui Y et al. *J. Lightwave Technol.* **40** 2503 (2022)
168. Zhou Z et al. *Light Sci. Appl.* **11** 15 (2022)

169. Zhou Z et al. *Opt. Lett.* **47** 5785 (2022)
170. Smith P W *Appl. Phys. Lett.* **19** 132 (1971)
171. Jensen R E, Tobin M S *Appl. Phys. Lett.* **20** 508 (1972)
172. Gonchukov S A et al. *Sov. J. Quantum Electron.* **5** 232 (1975); *Kvantovaya Elektron.* **2** 406 (1975)
173. Shi X et al. *Proc. SPIE* **6767** 67670H (2007)
174. Shi X et al. *Appl. Phys. B* **91** 377 (2008)
175. Shi X et al. *IEEE Photon. Technol. Lett.* **20** 650 (2008)
176. Bateman S A et al., in *CLEO*: *Science and Innovations, 2014, Postdeadline Paper Digest* (OSA Technical Digest) (Washington, DC: Optica Publ. Group, 2014) paper STh5C.10, https://doi.org/10.1364/CLEO_SI.2014.STh5C.10, online
177. Bateman S A et al., in *Advanced Photonics*: *Specialty Optical Fibers 2014* (OSA Technical Digest) (Washington, DC: Optica Publ. Group, 2014) paper SoM4B.3, online, https://doi.org/10.1364/SOF.2014.SoM4B.3
178. Love A L et al., in *CLEO*: *2015* (OSA Technical Digest) (Washington, DC: Optica Publ. Group, 2015) paper SF2F.4, online, https://doi.org/10.1364/CLEO_SI.2015.SF2F.4
179. Wadsworth W J, Love A L, Knight J C, in *Workshop on Specialty Optical Fibers and Their Applications* (OSA Technical Digest) (Washington, DC: Optica Publ. Group, 2015) paper WT1A.1, https://doi.org/10.1364/WSOF.2015.WT1A.1, online
180. Endo M, Walter R F (Eds) *Gas Lasers* (Optical Science and Engineering, Vol. 121) (Boca Raton, FL: CRC Press. Taylor and Francis, 2007)
181. Debord B et al., in *CLEO:2011 — Laser Applications to Photonic Applications* (OSA Technical Digest) (Washington, DC: Optica Publ. Group, 2011) paper CThD5, CD, https://doi.org/10.1364/CLEO_SI.2011.CThD5
182. Moisan M et al. *Rev. Phys. Appl.* **17** 707 (1982)
183. Gladyshev A et al. *Photonics* **9** 752 (2022)
184. Bufetov I A et al. *Dokl. Phys.* **68** 107 (2023); *Dokl. Ross. Akad. Nauk. Fiz. Tekh. Nauki* **509** 3 (2023)
185. Gladyshev A V et al. *Bull. Lebedev Phys. Inst.* **50** 403 (2023); *Kr. Soobshch. Fiz. FIAN* (9) 62 (2023)